Publication Year	2018
Acceptance in OA@INAF	2020-10-17T08:19:05Z
Title	A new method of measuring centre-of-mass velocities of radially pulsating stars from high-resolution spectroscopy
Authors	Britavskiy, N.; PANCINO, ELENA; Tsymbal, V.; ROMANO, Donatella; Fossati, L.
DOI	10.1093/mnras/stx2944
Handle	http://hdl.handle.net/20.500.12386/27871
Journal	MONTHLY NOTICES OF THE ROYAL ASTRONOMICAL SOCIETY
Number	474

Monthly Notices
of the
ROYAL ASTRONOMICAL SOCIETY

MNRAS **474,** 3344–3360 (2018) doi:10.1093/mnras/stx2944

A new method of measuring centre-of-mass velocities of radially pulsating stars from high-resolution spectroscopy

N. Britavskiy,[1,2,3★] E. Pancino,[4,5★] V. Tsymbal,[6] D. Romano[7] and L. Fossati[8]

[1]*Instituto de Astrofisica de Canarias, E-38205 La Laguna, Tenerife, Spain*
[2]*Universidad de La Laguna (ULL), Dpto. de Astrofísica, E-38206 La Laguna, Tenerife, Spain*
[3]*IAASARS, National Observatory of Athens, GR-15236 Penteli, Greece*
[4]*INAF – Osservatorio Astrofisico di Arcetri, Largo Enrico Fermi 5, 50125 Firenze, Italy*
[5]*ASI Science Data Center, Via del Politecnico snc, 01333 Roma, Italy*
[6]*Crimean Federal University, 295007, Vernadsky av. 4, Simferopol, Crimea*
[7]*INAF – Osservatorio Astronomico di Bologna, Via Gobetti 93/3, I-40129 Bologna, Italy*
[8]*Space Research Institute, Austrian Academy of Sciences, Schmiedlstrasse 6, A-8042 Graz, Austria*

Accepted 2017 November 10. Received 2017 November 9; in original form 2017 July 14

ABSTRACT

We present a radial velocity analysis of 20 solar neighbourhood RR Lyrae and three Population II Cepheid variables. We obtained high-resolution, moderate-to-high signal-to-noise ratio spectra for most stars; these spectra covered different pulsation phases for each star. To estimate the gamma (centre-of-mass) velocities of the programme stars, we use two independent methods. The first, 'classic' method is based on RR Lyrae radial velocity curve templates. The second method is based on the analysis of absorption-line profile asymmetry to determine both pulsational and gamma velocities. This second method is based on the least-squares deconvolution (LSD) technique applied to analyse the line asymmetry that occurs in the spectra. We obtain measurements of the pulsation component of the radial velocity with an accuracy of ± 3.5 km s^{-1}. The gamma velocity was determined with an accuracy of ± 10 km s^{-1}, even for those stars having a small number of spectra. The main advantage of this method is the possibility of obtaining an estimation of gamma velocity even from one spectroscopic observation with uncertain pulsation phase. A detailed investigation of LSD profile asymmetry shows that the projection factor p varies as a function of the pulsation phase – this is a key parameter, which converts observed spectral line radial velocity variations into photospheric pulsation velocities. As a by-product of our study, we present 41 densely spaced synthetic grids of LSD profile bisectors based on atmospheric models of RR Lyr covering all pulsation phases.

Key words: methods: data analysis – techniques: radial velocities – stars: oscillations – stars: variables: Cepheids – stars: variables: RR Lyrae.

1 INTRODUCTION

RR Lyraes are important tracers of galactic dynamics and evolution. Their high luminosity makes them good tracers for investigations of the Galactic halo (e.g. Kollmeier et al. 2009) and stellar systems outside the Milky Way (e.g. Stetson et al. 2014). Together with the proper motion, the centre-of-mass velocity (or gamma velocity, V_γ) of this type of star is thus a fundamental parameter that should be derived with the highest possible accuracy. With the *Gaia* satellite already measuring precise proper motions for thousands of variable stars in the Milky Way and beyond, the missing ingredient in a full determination of fundamental kinematic parameters for RR Lyrae stars is an estimate of gamma velocity.[1] Indeed, the uncertainties associated with the determination of gamma velocities of RR Lyrae stars constitute a long-standing problem, which also affects the accuracy of RR Lyraes as distance indicators (e.g. Benedict et al. 2011). Several studies have been devoted to this problem (Hawley & Barnes 1985; Jeffery et al. 2007; For, Sneden & Preston 2011; Sessar 2012; Nemec et al. 2013). Traditionally, the approach to derive the gamma velocity relies on a template radial

★ E-mail: britavskiy@iac.es (NB); pancino@arcetri.inaf.it (EP)

[1] *Gaia* is expected to measure radial velocities with errors of 1–15 km s^{-1}, depending on spectral type and brightness, for stars with $V < 16$ mag (Prusti et al. 2016), while proper motions will have errors ranging from a few μas yr^{-1} for bright stars down to a few 100 μas yr^{-1} for stars down to $V =$ 20 mag.

© 2017 The Author(s)
Published by Oxford University Press on behalf of the Royal Astronomical Society

Downloaded from https://academic.oup.com/mnras/article/474/3/3344/4762744 by INAF Trieste (Osservatorio Astronomico di Trieste) user on 01 October 2020

Table 1. Basic information for programme stars.

Star	RA (J2000) (h m s)	Dec. (J2000) (° ′ ″)	Type	V (mag)	ΔV (mag)	Epoch (JD 240 0000+)	Period (day)
DR And	01 05 10.71	+34 13 06.3	RRab *	11.65–12.94	1.29	51453.158583	0.5631300
X Ari	03 08 30.88	+10 26 45.2	RRab	11.28–12.60	1.32	54107.2779	0.6511681
TW Boo	14 45 05.94	+41 01 44.1	RRab	10.63–11.68	1.05	53918.4570	0.53226977
TW Cap	20 14 28.42	− 13 50 07.9	CWa	9.95–11.28	1.33	51450.139016	28.610100
RX Cet	00 33 38.28	− 15 29 14.9	RRab *	11.01–11.75	0.74	52172.1923	0.5736856
U Com	12 40 03.20	+27 29 56.1	RRc	11.50–11.97	0.47	51608.348633	0.2927382
RV CrB	16 19 25.85	+29 42 47.6	RRc	11.14–11.70	0.56	51278.225393	0.3315650
UZ CVn	12 30 27.70	+40 30 31.9	RRab	11.30–12.00	0.70	51549.365683	0.6977829
SW CVn	12 40 55.03	+37 05 06.6	RRab	12.03–13.44	1.41	51307.226553	0.4416567
AE Dra	18 27 06.63	+55 29 32.8	RRab	12.40–13.38	0.98	51336.369463	0.6026728
BK Eri	02 49 55.88	− 01 25 12.9	RRab	12.00–13.05	1.05	51462.198773	0.5481494
UY Eri	03 13 39.13	− 10 26 32.4	CWb	10.93–11.66	0.73	51497.232193	2.2132350
SZ Gem	07 53 43.45	+19 16 23.9	RRab	10.98–12.25	1.27	51600.336523	0.5011365
VX Her	16 30 40.80	+18 22 00.6	RRab *	9.89–11.21	1.32	53919.451	0.45536088
DH Hya	09 00 14.83	− 09 46 44.1	RRab	11.36–12.65	1.29	51526.426583	0.4889982
V Ind	21 11 29.91	− 45 04 28.4	RRab	9.12–10.48	1.36	47812.668	0.479601
SS Leo	11 33 54.50	− 00 02 00.0	RRab	10.38–11.56	1.18	53050.565	0.626335
V716 Oph	16 30 49.47	− 05 30 19.5	CWb	8.97–9.95	0.98	51306.272953	1.1159157
VW Scl	01 18 14.97	− 39 12 44.9	RRab	10.40–11.40	1.00	27809.381	0.5109147
BK Tuc	23 29 33.33	− 72 32 40.0	RRab	12.40–13.30	0.90	36735.605	0.5502000
TU UMa	11 29 48.49	+30 04 02.4	RRab	9.26–10.24	0.98	51629.148846	0.5576587
RV UMa	13 33 18.09	+53 59 14.6	RRab	9.81–11.30	1.49	51335.380433	0.4680600
UV Vir	12 21 16.74	+00 22 03.0	RRab *	11.35–12.35	1.00	51579.459853	0.5870824

Notes. Listed are coordinates (columns 2 and 3), variability class, where stars exhibiting the Blazhko effect (according to Skarka 2013) are marked by an asterisk (column 4), magnitude ranges (column 5), amplitude of the magnitude variation (column 6) and pulsation periods (column 8), taken from the General Catalog of Variable Stars (GCVS: Samus et al. 2007). The epochs of maximum light (column 7) were extracted from the ROTSE light curves (see Paper I for more details).

velocity curve, which is shifted and scaled to match the observed radial velocity at a few different phases (Liu 1991). This method becomes more accurate when observations covering several phases are available. In this work, we apply a method that allows us to estimate the gamma velocity of RR Lyrae stars from just a few observations obtained at random phases. The method is based on (i) investigations of the absorption-line profile asymmetry that occurs during radial pulsations and (ii) determination of the absolute value of the pulsation component using line-profile bisectors, taking limb-darkening effects carefully into account. We test our method on a sample of solar neighbourhood RR Lyraes investigated in a previous article (Pancino et al. 2015, hereinafter Paper I) and on densely spaced observations of RR Lyr (Fossati et al. 2014).

The article is organized as follows: in Section 2, we briefly review the observations and data reduction for our sample stars. In Section 3, we discuss the determination of the radial velocity and gamma velocity when applying the 'classic' method based on radial velocity curve templates. Section 4 presents our method of bisectors for the determination of gamma and pulsation velocities of RR Lyraes and compares the results with those from the classical approach. Moreover, we tested our method on high-resolution observations of RR Lyr. Section 5 presents the results of the analysis; Section 6 closes the article with a summary and conclusions. Appendix A presents an extensive library of synthetic bisectors that can be used to apply our proposed method to spectra of variable stars.

2 OBSERVATIONS AND DATA REDUCTION

The analysed sample consists of 20 RR Lyr stars and three Population II Cepheids. The stars were observed as part of different programmes with the Spettrografo ad Alta Risoluzione Galileo (SARG) (Gratton et al. 2001) echelle spectrograph at the Telescopio Nazionale Galileo (TNG: La Palma, Spain) and the Ultraviolet and Visual Echelle Spectrograph (UVES: Dekker et al. 2000) at the European Southern Observatory (ESO) Very Large Telescope (VLT: Paranal, Chile). Furthermore, additional archival spectra were retrieved from the ESO archive. The resolving power of the spectra obtained with SARG is $R = \lambda/\delta\lambda \approx 30\,000$, with an average signal-to-noise ratio (S/N) $\approx$ 50–100 and spectral coverage from 4000–8500 Å. The UVES spectra have a higher resolving power, $R \approx$ 47 000, and S/N $\approx$ 70–150 and cover the wavelength range from 4500–7500 Å. The observations were performed at random pulsation phases, generally three times for each star; however, for some stars we have more then three observations or just one observation. Table 1 presents some general information about the programme stars.

A full description of the observations and reduction process, including determination of the fundamental parameters of the sample stars, is presented in Paper I. Briefly, SARG spectra were reduced with standard IRAF[2] tasks in the *echelle* package, including bias and flat-field correction, spectral tracing, extraction, wavelength calibration and continuum normalization. The typical root-mean-square (r.m.s.) deviation of wavelength calibration line centroids from the two-dimensional fitted calibration polynomials was close to 0.03 Å. Sky absorption lines (telluric bands of O_2 and H_2O) were removed using the IRAF task *telluric* with the help of our own library

[2] IRAF (http://iraf.noao.edu/) is distributed by the National Optical Astronomical Observatory, which is operated by the Association of Universities for Research in Astronomy (AURA) under cooperative agreement with the National Science Foundation.

Downloaded from https://academic.oup.com/mnras/article/474/3/3344/4762744 by INAF Trieste (Osservatorio Astronomico di Trieste) user on 01 October 2020

of observed spectra. UVES spectra were reduced with the UVES pipeline (Ballester et al. 2000) as part of the service observations and include similar steps to the ones described for SARG.

The data set from Paper I was complemented by the densely spaced observations of RR Lyrae along the pulsation cycle described by Fossati et al. (2014).

3 GAMMA VELOCITY OF PULSATING STARS

From an observational point of view, the gamma velocity, V_γ, can be described using the following equation:

$$V_\gamma = v_{\rm obs} + v_\odot - v_{\rm puls}, \quad (1)$$

where $v_{\rm obs}$ is the observed velocity of the star along the line of sight, $v_\odot$ is the heliocentric correction and $v_{\rm puls}$ is the pulsation velocity of the radially pulsating star. We will see in the following sections that the determination of $v_{\rm puls}$ requires a treatment of limb-darkening effects, generally included in the form of a *projection factor*. The sum $v_{\rm obs} + v_\odot$ is the heliocentric radial velocity of the star, $v_{\rm rad}$, at any given phase in the pulsation cycle. In other words, the determination of the gamma velocity of pulsating stars such as RR Lyraes and Cepheids requires – in principle – the determination of two quantities: (i) the observed radial velocity (reported to the heliocentric reference) and (ii) the pulsation component at the moment of the observation or, better, at the specific pulsation phase of the observations (corrected for limb-darkening effects).

In the next subsections we apply the most widely used method for deriving the gamma velocity to the sample described in Section 2. The resulting measurements (reported in Table 2) are then used as reference values to test the method based on bisectors (Section 4).

3.1 Measurement of $v_{\rm obs}$ using cross-correlation

We first measured the radial velocity of our sample spectra using the classical cross-correlation method, implemented in the IRAF *fxcor* task and based on the standard Tonry & Davis (1979) algorithm. We cross-correlated the observed spectra with synthetic spectra generated with the latest modified version (15 March 2013) of the STARSPSYNTHV package, a local thermodynamic equilibrium (LTE) spectral synthesis code developed by Tsymbal (1996), which uses ATLAS9 (Kurucz 1993) grids of stellar atmosphere models. We adopted the following typical atmospheric parameters of RR Lyr stars for the synthetic spectrum generation: $T_{\rm eff} = 6250$ K, $\log g = 2.5$ dex, $v_{\rm mic} = 2.0\,{\rm km\ s^{-1}}$, chosen as typical values at quiescent phases along the RR Lyr star pulsation cycle from Paper I. Then we convolved the synthetic spectrum with a Gaussian to reproduce the spectral resolution of the observed spectra (Section 2). We performed a cross-correlation analysis for all spectra in the wavelength range 5100–5400 Å, where several prominent, not blended, Ti and Fe lines are present. We remark that the low metallicity of RR Lyrae stars leads to limited line blending.

The resulting radial velocity measurements derived by the cross-correlation method ($v_{\rm obs}^{\rm Xcor}$) and their errors ($\delta v_{\rm obs}^{\rm Xcor}$), as estimated by the position and full width at half-maximum of the cross-correlation peak, are reported in Table 2, along with their heliocentric corrections, $v_\odot$.

3.2 Measurement of V_γ using velocity curve templates

We used the classical radial velocity curve template approach to obtain the final $V_\gamma^{\rm Xcor}$, which is also reported in Table 2. The method relies on the use of an appropriate template radial velocity curve, which is fitted to the observed radial velocity points to obtain the systemic or gamma velocity of the variable star. In our sample, we have RRab Lyrae (fundamental mode pulsator) and RRc Lyrae (first overtone pulsator) stars. The former present asymmetric light curves with large radial velocity and magnitude ($\delta V \approx 0.5$–2 mag) variations. The latter, instead, have relatively symmetric light curves with smaller magnitude and radial velocity variations. The physics of RRc-type variability is still poorly understood (see conclusions in Moskalik et al. 2015), mainly because of the presence of several radial and non-radial pulsation modes. Thus, in our analysis for RRc-type stars we used as a reference the average radial velocity curves of well-known RRc Lyraes with similar radial velocity amplitudes. For a few of our RRab stars, we could rely on existing radial velocity curves from the literature: V Ind (Clementini, Cacciari & Lindgren 1990); X Ari (Jones et al. 1987), TU Uma (Liu & Janes 1989) and U Com (Beers et al. 2000). For these stars, the Baade–Wesselink (B–W) method was applied in the literature, thus reliable radial velocity curves exist for this sample. We noted that the typical amplitudes of these curves were all around $60\,{\rm km\ s^{-1}}$. For the RRc-type variables in our sample, we used the velocity curves of DH Peg (Jones, Carney & Latham 1988) and YZ Cap (Cacciari et al. 1987), both with amplitudes of $\simeq 25\,{\rm km\ s^{-1}}$. For the three Cepheids, TW Cap, V716 Oph and UY Eri, we used the radial velocity curve of W Vir (Sanford 1952).

For the remaining stars, we reconstructed synthetic radial velocity curves following Liu (1991), who provided both a template radial velocity curve for RRab stars and a correlation between the amplitudes of light curves and radial velocity curves, based on a large sample of RR Lyrae observations. We used the magnitude ranges reported in Table 1 to obtain radial velocity amplitudes with equation (1) in Liu (1991). We then divided the amplitude obtained by an average projection factor of 1.3 (see also Section 4.5) and scaled the template curve appropriately. We next adjusted the template curve to our measured radial velocities – an example of this procedure is shown in Fig. 1 (top panel) for V Ind, which has several spectra at different phases. The final gamma velocity is obtained as an average of the (scaled and shifted) radial velocity curve that fits the observational points.

The typical uncertainties connected to the use of this method depend on several factors. As discussed by Liu (1991, see also Jeffery et al. 2007), the error in the normalization of the radial velocity curve is about $3\,{\rm km\ s^{-1}}$, to which one has to add the individual radial velocity uncertainties (Table 2). Additionally, whenever an observed radial velocity curve was available in the literature, we repeated the analysis with the observed curve and compared the results. In each case, the results obtained with the two methods were comparable – i.e. no systematic differences were found – so we used a weighted average of the results obtained with the template and observed curve.

4 BISECTORS METHOD

The classical method described above provides good results when good phase sampling is available or, in the case of few observations, when the phase of the observations is well known. In this section, we discuss an alternative method for determination of the gamma velocity, based on the asymmetry of line profiles in pulsating stars, which vary along the pulsation cycle and thus can also be used to infer the pulsational velocity. This method, hereafter referred to as the *bisectors method* for brevity, allows for an estimate of the gamma velocity of pulsating stars with a sparse phase sampling and works even with just one observation, albeit with a slightly larger uncertainty. In the literature, this method was mentioned by several

Downloaded from https://academic.oup.com/mnras/article/474/3/3344/4762744 by INAF Trieste (Osservatorio Astronomico di Trieste) user on 01 October 2020

Table 2. Radial and gamma velocities of programme stars, derived with the classical cross-correlation and radial velocity curve approach.

Star	Inst.	Exp	Phase	$v_{\rm obs}^{\rm Xcor}$ (km s^{-1})	$\delta v_{\rm obs}^{\rm Xcor}$ (km s^{-1})	$v_{\odot}$ (km s^{-1})	$v_{\rm rad}^{\rm Xcor}$ (km s^{-1})	$V_{\gamma}^{\rm Xcor}$ (km s^{-1})	$\delta V_{\gamma}^{\rm Xcor}$ (km s^{-1})
DR And	SARG	1	0.63	− 119.67	0.25	17.59	− 102.08	− 109.7	3.0
	SARG	2	0.69	− 116.33	0.26	17.53	− 98.80	− 125.4	3.1
	SARG	3	0.31	− 118.91	0.12	6.91	− 112.00	− 123.1	3.4
X Ari	APO	1	0.19	− 23.25	0.26	− 27.19	− 50.44	− 36.1	3.6
TW Boo	SARG	1	0.61	− 83.20	0.12	3.11	− 80.09	− 101.1	1.5
	SARG	2	0.65	− 80.67	0.13	3.11	− 77.56	− 100.4	1.6
	SARG	3	0.69	− 79.87	0.13	3.07	− 76.81	− 100.3	1.4
TW Cap	UVES	1	0.54	− 46.60	0.13	− 15.68	− 62.28	− 72.3	5.0
RX Cet	SARG	1	0.51	− 75.79	0.22	− 4.34	− 80.13	− 93.7	3.1
U Com	SARG	1	0.06	− 13.46	0.17	− 5.55	− 19.01	− 7.8	3.2
	SARG	2	0.14	− 8.42	0.14	− 5.58	− 14.00	− 5.6	3.2
	SARG	3	0.21	− 4.34	0.11	− 5.61	− 9.95	− 7.1	3.2
RV CrB	SARG	1	0.35	− 147.40	0.19	13.70	− 133.70	− 138.3	3.6
	SARG	2	0.42	− 146.20	0.28	13.66	− 132.54	− 139.8	3.7
	SARG	3	0.48	− 147.40	0.70	13.62	− 133.78	− 142.4	3.7
SW CVn	SARG	2	0.21	19.19	0.30	− 7.80	11.39	24.0	3.9
	SARG	3	0.28	17.44	0.49	− 7.86	9.58	16.5	3.1
UZ CVn	SARG	1	0.04	− 39.35	0.18	− 8.70	− 47.44	− 19.6	4.1
	SARG	2	0.08	− 33.10	0.11	− 8.77	− 41.52	− 17.1	3.5
	SARG	3	0.13	− 29.41	0.12	− 8.84	− 37.90	− 18.2	4.0
AE Dra	SARG	1	0.05	− 309.69	0.18	6.03	− 303.66	− 275.7	1.7
	SARG	2	0.10	− 304.91	0.17	5.99	− 298.92	− 275.3	1.7
BK Eri	UVES	1	0.04	95.33	0.69	− 27.12	68.20	98.6	1.7
	UVES	2	0.20	109.29	0.16	− 27.03	82.26	97.2	1.5
	UVES	3	0.14	102.80	0.21	− 27.04	75.76	95.8	1.7
	UVES	4	0.51	137.82	0.08	− 26.83	110.99	96.3	1.8
UY Eri	SARG	1	0.38	129.09	0.24	21.16	150.25	151.9	5.0
SZ Gem	SARG	1	0.50	309.44	0.23	26.93	336.37	321.6	3.0
VX Her	SARG	1	0.86	− 370.87	0.13	18.47	− 351.96	− 340.1	5.3
	SARG	2	0.05	− 391.85	0.98	18.43	− 373.33	− 402.4	4.8
DH Hya	UVES	1	0.79	389.03	0.18	− 24.17	364.86	336.3	4.5
	SARG	2	0.71	381.25	0.15	− 20.06	361.18	334.1	5.2
	SARG	3	0.79	385.19	0.26	− 20.17	365.02	334.3	4.3
V Ind	UVES	1	0.19	175.00	0.22	6.03	181.03	194.9	4.6
	UVES	2	0.29	204.00	0.09	− 12.13	191.87	196.1	3.3
	FEROS	1	0.46	208.00	0.08	3.31	211.31	197.1	3.1
	FEROS	2	0.60	217.00	0.11	3.20	220.20	198.3	3.0
	FEROS	3	0.63	219.00	0.11	3.18	222.18	198.0	3.1
	HARPS	1	0.67	221.00	0.24	2.77	223.77	196.3	3.0
	HARPS	2	0.69	222.00	0.24	2.77	224.77	197.6	3.0
	HARPS	3	0.72	223.00	0.26	2.74	225.74	198.2	3.0
	HARPS	4	0.38	201.00	0.17	2.69	203.69	198.9	3.2
	HARPS	5	0.41	204.00	0.21	2.69	206.69	199.3	3.8
	HARPS	6	0.74	224.00	0.28	2.34	226.34	198.0	4.9
	HARPS	7	0.77	223.00	0.33	2.00	225.00	196.2	6.1
	HARPS	8	0.80	222.00	0.33	2.00	224.00	194.4	9.8
	HARPS	9	0.83	222.00	0.27	1.90	223.90	193.2	8.4
	HARPS	10	0.87	221.78	0.21	1.87	223.65	194.5	7.5
SS Leo	UVES	1	0.06	156.83	0.23	− 20.77	136.06	165.4	4.1
	UVES	2	0.07	155.53	0.25	− 20.79	134.74	162.2	3.9
V716 Oph	UVES	1	0.08	− 307.06	0.11	− 28.25	− 335.31	− 310.8	5.0
VW Scl	UVES	1	0.71	86.85	0.12	− 25.91	67.02	40.3	3.2
	UVES	2	0.23	57.41	0.09	− 25.83	31.58	41.0	3.0
	UVES	3	0.32	65.86	0.06	− 25.59	40.27	41.2	3.1
	UVES	4	0.15	47.69	0.15	− 25.41	22.28	42.2	3.0
	UVES	5	0.05	37.76	0.37	− 25.63	12.13	37.7	3.2
BK Tuc	UVES	1	0.17	162.49	0.12	− 2.52	159.97	167.4	3.1
	UVES	2	0.26	162.25	0.15	− 2.57	159.68	174.4	3.1
	UVES	3	0.15	160.86	0.11	− 2.86	158.00	167.4	3.1
TU UMa	SARG	1	0.45	122.65	0.10	− 13.15	109.50	99.4	3.0
RV Uma	SARG	1	0.62	− 171.26	0.16	− 5.61	− 176.87	− 200.1	3.9
	SARG	2	0.66	− 167.39	0.14	− 5.64	− 173.03	− 198.8	3.7
	SARG	3	0.71	− 164.40	0.15	− 5.67	− 170.07	− 196.2	5.9
UV Vir	UVES	1	0.87	74.20	0.18	− 16.58	57.62	99.4	3.0

Downloaded from https://academic.oup.com/mnras/article/474/3/3344/4762744 by INAF Trieste (Osservatorio Astronomico di Trieste) user on 01 October 2020

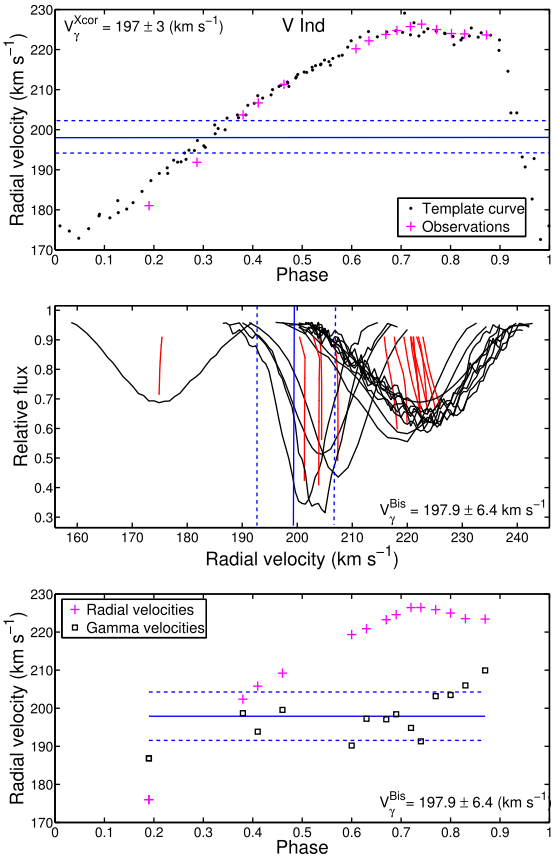

Figure 1. Examples of gamma velocity estimates for V Ind, obtained with a reference radial velocity curve (Clementini et al. 1990, top panel; see also Section 3) and with the bisectors method (middle and bottom panels; see Section 4), which has several spectra obtained at different phases. In the middle panel we present the individual LSD profiles together with their bisectors, while the bottom panel shows the observed radial velocities (crosses) and derived individual values of gamma velocity (boxes). The resulting gamma velocity is marked by a solid line in all panels, with dashed lines showing the errors associated with each determination.

authors (e.g. Hatzes 1996; Gray 2010). Other authors (e.g. Sabbey et al. 1995; Nardetto et al. 2008, 2013) use the *Gaussian asymmetry coefficient* to estimate line asymmetries and perform the same task; however, the bisectors method allows for a more detailed study of the line profile, i.e. study of line asymmetries and $v_{\rm puls}$ variations at different depths inside the stellar atmosphere. On the other hand, the bisectors method is in general more sensitive to spectral quality, i.e. the S/N ratio, spectral resolution and line crowding and blending.

To derive average line profiles, we use the least-squares deconvolution (LSD) method (Donati et al. 1997), which infers a very high S/N ratio line profile for each spectrum from the profiles of many observed absorption lines, under the assumption that the vast majority of lines have the same shape and that different line components add up linearly (Kochukhov, Makaganiuk & Piskunov 2010). Depending on the number of lines used, the reconstructed LSD profile can have an extremely high S/N ratio, rarely attainable with RR Lyrae observations on single lines. The problem with RR Lyrae is that it is difficult to make long-exposure observations without avoiding the line-smearing effect; as a result, it limits the S/N of obtained spectra. The original LSD method by Donati et al. (1997) was modified and extended to different applications by several authors (e.g. Kochukhov, Makaganiuk & Piskunov 2010; Van Reeth, Tkachenko & Tsymbal 2013; Tkachenko et al. 2013, among others). We used the Tkachenko et al. (2013) implementation (see next section) and our workflow can be outlined as follows.

(i) We compute the LSD profile of each observed spectrum; this also allows for an independent estimate of $v_{\rm obs}$ (Section 4.1).

(ii) We compute a theoretical library of LSD profiles (Appendix A), predicting the line-profile asymmetries at each pulsation phase, and compute the bisectors of each of the profiles; the theoretical bisectors library is made available in the electronic version of this article and can be used to derive $v_{\rm obs}$ and V_γ for RR Lyrae observations obtained at unknown or poorly determined phases.

(iii) we compute the bisector of the observed LSD line profile and compare it with those in our theoretical library, to determine which pulsation velocity corresponds to the observed asymmetry of the LSD bisector (Section 4.2); in our computation, we implement a full description of limb-darkening effects (Section 4.5).

Once the observed and pulsational components are known, the gamma velocity can be obtained trivially from equation (1).

4.1 Measurement of $v_{\rm obs}$ using LSD profiles

The LSD method for computing the line profile requires a list of spectral lines, specified by their central peak position and depth or central intensity, which is generally referred to as a *line mask*. The whole spectrum is thus modelled as the convolution of an ideal line profile (assumed identical for all lines) with the actual pattern of lines from the mask. The LSD line profile is obtained by deconvolution from the line pattern, given an observed spectrum. Because the whole computation takes place in velocity space, the actual LSD profile carries the $v_{\rm obs}$ information, in our particular case determined as the centre of mass of the profile (Hareter et al. 2008; Kochukhov et al. 2010).

We built our line mask from the same line list that was used for our abundance analysis in Paper I and is described there in detail. Briefly, we selected all isolated lines that were measured well (errors below 20 per cent) in at least three of the available spectra. For the line measurements we used DAOSPEC (Stetson & Pancino 2008). After the abundance analysis, performed with GALA (Mucciarelli et al. 2013), all lines that gave systematically discrepant abundances or were systematically rejected because of their strengths or relative errors were purged from the list. The final line list consisted of 352 isolated lines belonging to nine different chemical species (see Paper I).

We used the LSD code described by Tkachenko et al. (2013), which is a generalization of the original method by Donati et al. (1997). We applied the method in the wavelength range 5100–5400 Å, which contains 155 of the above-mentioned lines from Paper I.[3]

Fig. 2 displays the results of our computation. The resulting $v_{\rm obs}^{\rm LSD}$ values are reported in Table 3, along with their errors, $\delta v_{\rm obs}^{\rm LSD}$. To evaluate the final errors, we evaluated different possible error sources and summed them in quadrature. A first uncertainty is the difference between the minimum of the LSD profile and its centre of mass, typically in the range 0.5–1 km s^{-1}. Since the line selection can have an impact on the line profiles, we repeated our measurements with three different line lists – using lines with depth lower than 65, 75 and 85 per cent of the continuum level – and used

[3] It is worth emphasizing that the wavelength range 5100–5400 Å was used for both the cross-correlation analysis described in Section 3.1 and the LSD analysis, for consistency.

Downloaded from https://academic.oup.com/mnras/article/474/3/3344/4762744 by INAF Trieste (Osservatorio Astronomico di Trieste) user on 01 October 2020

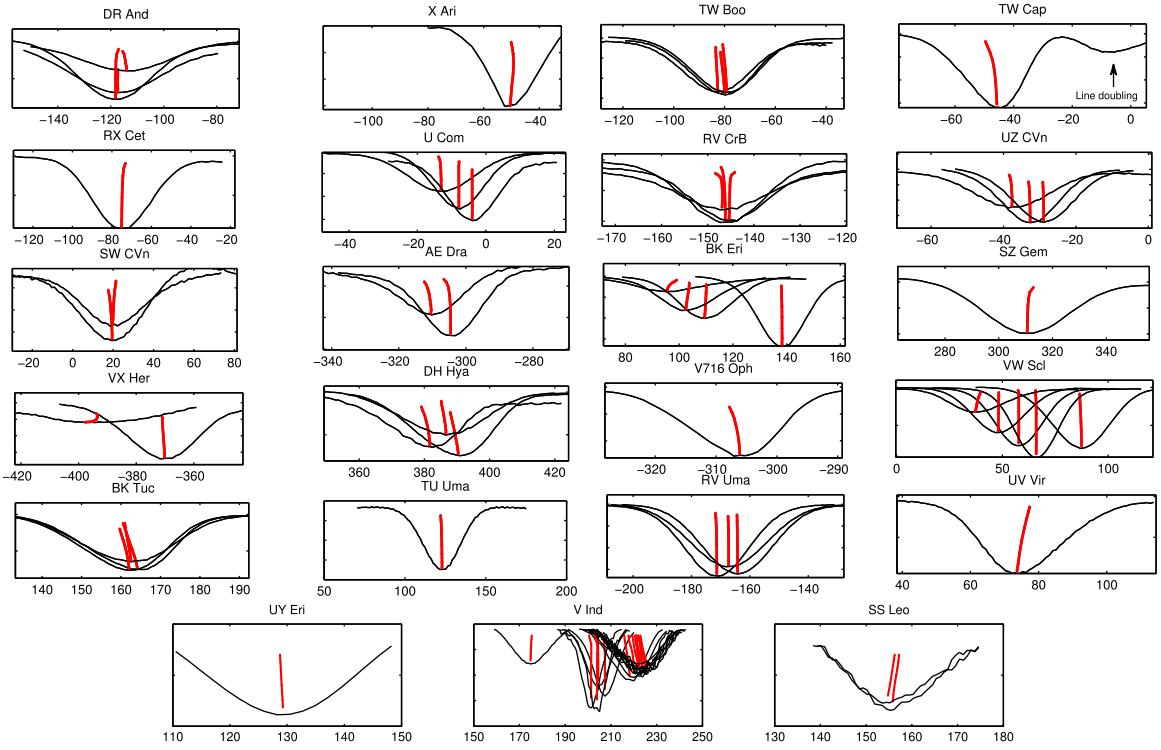

Figure 2. LSD profiles (black lines) and bisectors (red lines) for all sample spectra. The x-axis gives the velocity in km s^{-1}.

the dispersion in the resulting radial velocity as the uncertainty caused by the line selection procedure, obtaining values typically around 0.5 km s^{-1}. We note that V Ind has more observations along the pulsation cycle than other stars in the sample, which makes it the perfect test case for our method. The LSD profiles for V Ind are displayed in the lower panel of Fig. 1, where the variation of the line shape with phase is clearly visible in both the line-shape asymmetry and bisectors slope.

Finally, we compared the $v_{\rm obs}$ values obtained with the classical cross-correlation method with those obtained with the LSD profile method (Fig. 3) and found an extremely good agreement, with an average offset of 0.3 km s^{-1} and a spread generally below 1 km s^{-1}, which is compatible with the individual error estimates of the two methods.

The star TW Cap in our sample deserves particular attention. This star is a well-known peculiar Type II Cepheid (Maas, Giridhar & Lambert 2007). The LSD profile shows a double minimum (see Fig. 2), hinting at the line-doubling phenomenon. Moreover, a double emission peak in Hβ is clearly visible in our spectrum. Wallerstein (1958) was the first to report double lines in the spectra of TW Cap. These features could be explained by the existence of supersonic shock waves in the atmosphere at our observation phase ($\phi = 0.54$). The same phenomenon is observed during shock phases in the spectra of RR Lyr (Chadid, Vernin & Gillet 2008).

4.2 Measurement of $v_{\rm puls}$ using line bisectors

For a quantitative characterization of the LSD profile asymmetry, we used the bisector technique, which is a widely used diagnostic of line asymmetries (e.g. Gray 2010). For each LSD profile, we computed the bisector of eight equally spaced depth layers, starting from a level of relative flux equal to 0.91 and reaching to the bottom of the line profile, at a flux level varying from 0.46–0.77, depending on the spectrum. The upper layer of the LSD profile, however, was found to be relatively uncertain, partly because we restricted ourselves to a small wavelength region and partly because of the paucity of lines in some of the analysed spectra, caused by the low metallicity. Therefore, in the following, only the lowest seven layers will be employed (with relative flux below 0.85). The observed bisectors are shown in Fig. 2, together with the computed LSD profiles.

To derive the pulsational velocity, $v_{\rm puls}$, we compared the observed bisectors with a library of theoretical bisectors specifically computed for the programme stars. The library is described in detail in Appendix A and is publicly available in the electronic version of this article and at the Centre de Données astronomiques de Strasbourg (CDS). One grid of theoretical LSD profiles and bisectors is shown in Fig. 4, as an example. To find the best-matching theoretical bisector for each observed bisector, we minimized the quadratic difference between the two,

$$\sqrt{\sum_{n=1}^{n=7}(Bis_n^{\rm Obs} - Bis_n^{\rm Templ})^2},$$

where 7 is the number of bisector points we take into account in the analysis (see above) and $Bis_n^{\rm Obs}$ and $Bis_n^{\rm Templ}$ are the values of the bisector evaluated at each layer of the observed and theoretical LSD profiles, respectively. In those cases where the exact phase of the observation is unknown, one can proceed in two steps. First, a blind comparison with the entire library is performed, providing an indication of the phase, and then a second iteration with the appropriate bisectors for that phase can be run.

Fig. 5 illustrates, as an example, the best fit obtained with this technique for our first exposure of V Ind (see Table 3).

Downloaded from https://academic.oup.com/mnras/article/474/3/3344/4762744 by INAF Trieste (Osservatorio Astronomico di Trieste) user on 01 October 2020

Table 3. Radial, pulsational and gamma velocities of programme stars, derived with the LSD profile and the bisectors method.

Star	Inst.	Exp	Phase	$v_{\rm obs}^{\rm LSD}$ (km s^{-1})	$\delta v_{\rm obs}^{\rm LSD}$ (km s^{-1})	$v_{\rm rad}^{\rm LSD}-V_\gamma^{\rm Bis}$ (km s^{-1})	$v_{\rm puls}^{\rm Bis}$ (km s^{-1})	$\delta v_{\rm puls}^{\rm Bis}$ (km s^{-1})	$V_\gamma^{\rm Bis}$ (km s^{-1})	$\delta V_\gamma^{\rm Bis}$ (km s^{-1})
DR And	SARG	1	0.63	− 119.8	0.5	5.2	5	5.0	− 107.4	5.9
	SARG	2	0.69	− 115.0	0.9	16.8	20	0.6	− 114.2	1.5
	SARG	3	0.31	− 118.6	0.5	− 2.6	− 5	1.0	− 109.0	3.3
X Ari	APO	1	0.19	− 51.1	1.3	− 34.3	− 43	2.0	− 43.9	2.6
TW Boo	SARG	1	0.61	− 83.0	1.7	8.1	10	5.0	− 88.0	5.4
	SARG	2	0.65	− 80.3	1.2	11.4	13	1.5	− 88.6	2.1
	SARG	3	0.69	− 79.2	0.2	14.3	17	1.9	− 90.4	2.2
TW Cap	UVES	1	0.54	− 46.1	1.1	25.4	30	1.0	− 87.2	1.8
RX Cet	SARG	1	0.51	− 75.5	0.5	− 11.8	− 17	2.1	− 68.0	2.4
U Com	SARG	1	0.87	− 13.5	0.1	4.3	4	2.0	− 23.3	3.7
	SARG	2	0.95	− 8.1	0.2	7.8	1	1.0	− 15.9	1.5
	SARG	3	0.02	− 4.0	1.1	3.2	3	5.0	− 12.8	6.1
RV CrB	SARG	1	0.35	− 146.5	0.4	5.2	5	3.8	− 137.9	4.9
	SARG	2	0.42	− 145.3	0.8	− 0.1	− 2	6.3	− 131.5	7.1
	SARG	3	0.48	− 147.3	0.2	− 3.1	− 6	2.5	− 130.5	2.7
SW CVn	SARG	2	0.21	17.8	2.0	− 0.1	− 2	3.3	10.1	5.4
	SARG	3	0.28	17.7	1.0	− 7.7	− 12	2.9	17.6	3.2
UZ CVn	SARG	1	0.04	− 38.1	0.2	− 0.1	− 2	5.0	− 46.0	5.9
	SARG	2	0.08	− 32.9	0.2	14.2	17	0.5	− 55.9	1.2
	SARG	3	0.13	− 29.0	0.1	7.9	10	0.5	− 45.7	1.2
AE Dra	SARG	1	0.05	− 309.3	0.6	11.3	13	1.0	− 314.5	1.6
	SARG	2	0.10	− 304.6	0.4	9.7	11	5.0	− 308.3	5.1
BK Eri	UVES	1	0.04	95.0	0.1	− 14.3	− 17	1.5	82.2	1.9
	UVES	2	0.20	109.2	0.1	− 11.8	− 16	0.5	93.9	1.2
	UVES	3	0.14	102.3	0.7	− 13.3	− 19	1.0	88.6	1.6
	UVES	4	0.51	138.1	0.2	2.7	1	3.0	108.6	4.3
UY Eri	SARG	1	0.38	129.3	1.1	4.4	4	4.5	146.1	5.7
SZ Gem	SARG	1	0.50	310.2	0.2	− 8.9	− 13	3.9	346.0	4.1
VX Her	SARG	1	0.86	− 370.7	0.8	7.1	8	5.0	− 359.3	5.2
	SARG	2	0.05	− 397.3	0.9	− 34.0	− 43	2.0	− 344.9	2.4
DH Hya	UVES	1	0.79	390.1	1.2	27.9	33	1.5	338.1	2.1
	SARG	2	0.71	381.8	0.5	24.2	29	5.0	337.5	5.1
	SARG	3	0.79	385.8	1.1	− 2.7	− 5	8.0	368.5	8.7
V Ind	UVES	1	0.19	174.9	0.1	− 11.8	− 17	0.6	192.7	1.3
	UVES	2	0.29	204.4	0.1	− 1.9	− 4	3.5	194.2	4.7
	FEROS	1	0.46	207.5	0.2	5.2	5	3.1	205.6	4.5
	FEROS	2	0.60	218.4	1.6	31.3	38	0.5	190.3	2.0
	FEROS	3	0.63	220.0	0.1	15.8	19	5.0	207.4	7.1
	HARPS	1	0.67	223.1	0.6	36.1	43	0.5	189.7	1.3
	HARPS	2	0.69	224.1	1.3	36.1	43	0.5	190.8	1.8
	HARPS	3	0.72	225.6	0.7	14.3	17	1.0	208.4	1.9
	HARPS	4	0.38	201.3	0.2	− 10.7	− 16	3.5	214.7	3.6
	HARPS	5	0.41	203.9	1.2	− 7.2	− 11	1.9	213.9	2.4
	HARPS	6	0.74	226.5	1.0	36.1	43	0.5	192.7	1.5
	HARPS	7	0.77	223.7	1.3	15.7	19	0.5	210.0	1.7
	HARPS	8	0.80	222.5	1.2	19.5	24	1.0	205.0	1.9
	HARPS	9	0.83	222.5	0.5	22.3	27	3.7	202.1	3.8
	HARPS	10	0.87	222.3	0.2	18.4	22	2.1	205.8	2.4
SS Leo	UVES	1	0.06	155.7	0.5	− 23.2	− 32	0.5	158.1	1.1
	UVES	2	0.07	154.6	1.1	− 23.1	− 31	2.6	156.8	3.0
V716 Oph	UVES	1	0.08	− 305.8	1.2	36.0	43	0.5	− 370.1	1.7
VW Scl	UVES	1	0.71	87.2	1.5	5.2	4	0.5	56.1	3.8
	UVES	2	0.23	57.4	0.7	− 0.7	− 1	2.5	32.3	4.0
	UVES	3	0.32	65.8	0.4	1.2	0	5.0	39.1	5.8
	UVES	4	0.15	47.6	0.3	− 7.3	11	3.5	29.4	3.6
	UVES	5	0.05	36.9	0.5	− 13.1	− 17	1.2	24.4	1.7
BK Tuc	UVES	1	0.17	164.3	0.2	33.8	40	1.7	128.0	2.0
	UVES	2	0.26	162.7	0.8	19.1	23	4.3	141.1	4.5
	UVES	3	0.15	162.1	1.0	25.6	31	2.2	133.7	2.6
TU UMa	SARG	1	0.45	122.9	0.6	3.2	3	2.5	106.5	4.0
RV Uma	SARG	1	0.62	− 171.6	0.1	2.7	1	1.5	− 179.9	3.4
	SARG	2	0.66	− 167.5	2.0	1.2	0	5.0	− 174.3	6.5
	SARG	3	0.71	− 164.2	0.4	1.2	0	5.0	− 171.1	5.8
UV Vir	UVES	1	0.87	73.4	0.2	− 23.4	− 32	2.0	80.8	2.3

Downloaded from https://academic.oup.com/mnras/article/474/3/3344/4762744 by INAF Trieste (Osservatorio Astronomico di Trieste) user on 01 October 2020

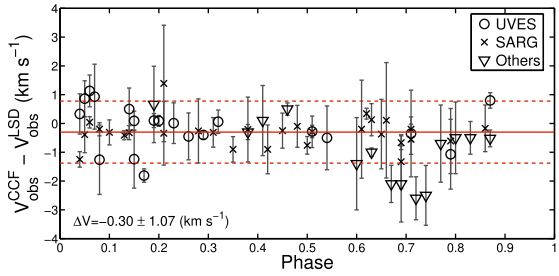

Figure 3. Differences between radial velocity estimates derived with the cross-correlation method, $v_{\rm obs}^{\rm Xcor}$, and with the LSD profile method, $v_{\rm obs}^{\rm LSD}$. Observations from different spectrographs are labelled respectively.

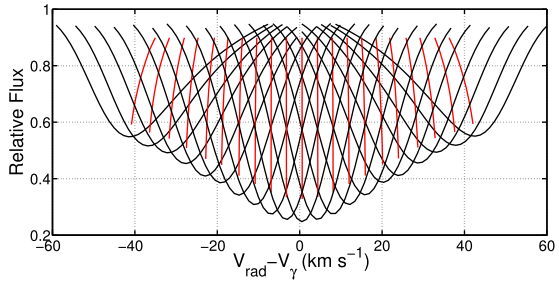

Figure 4. Example of LSD profiles and bisectors computed from model spectra of RR Lyrae (corresponding to $\phi = 0.213$, or spectrum number 087 in Fossati et al. 2014) with pulsation velocities from −50 to +50 km s^{-1} with a step of 5 km s^{-1}.

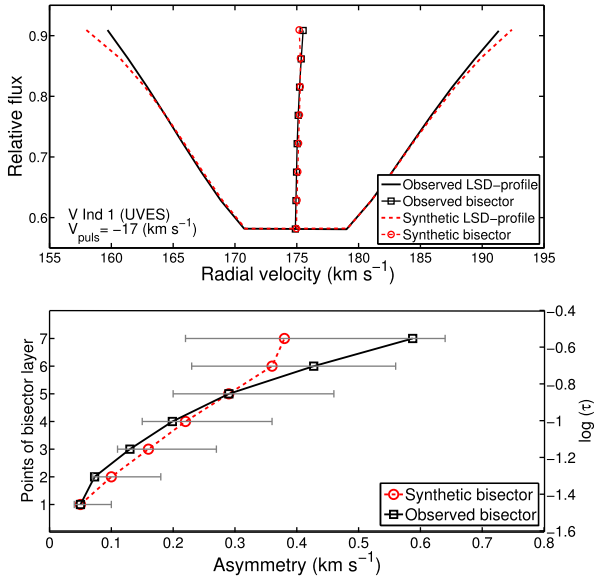

Figure 5. Comparison of observed (solid) and best-fitting theoretical (dashed) LSD profiles (top panel) and bisectors (bottom panel) for our first V Ind spectrum ($\phi = 0.19$; see Table 3). The best fit corresponds to $v_{\rm puls} = -17 \pm 1$ km s^{-1}. The grey error bars in the bottom panel correspond to the estimated errors in the method for determining $v_{\rm puls}$, i.e. 1 km s^{-1}. The optical depth scale on the right ordinate axis was computed from synthetic spectra built with the atmospheric parameters derived in Paper I: $T_{\rm eff}$ = 7000 K, $\log g$ = 2.3 dex, $v_{\rm mic}$ = 1.6 km s^{-1} and [Fe/H] = −1.3 dex. The divergence between the observed and theoretical bisectors in layer 7 is caused by the lower S/N ratio of the LSD profile in this layer (see text for details). While the model bisector does not follow the shape of the observed ones exactly, the two agree reasonably well within the uncertainties.

4.3 A test on RR Lyr

In order to test the method, we applied it to the prototype of the RR Lyrae class: RR Lyr itself. We used 41 high-resolution (R = 60 000), high signal-to-noise ratio (100–300) spectra of RR Lyr taken along the whole pulsation cycle analysed by Kolenberg et al. (2010) and Fossati et al. (2014). In these articles, the authors determined the phase-dependent atmospheric parameters of RR Lyr, based on which we compute the synthetic spectra and theoretical bisectors for each of the 41 observations of RR Lyr. Thus, the number and IDs of each spectrum of RR Lyr from Fossati et al. (2014) are the same as the number of theoretical stellar atmosphere models we used for constructing the grid of synthetic bisectors (see Appendix A). The good phase sampling allows us to test the method thoroughly over the whole pulsation cycle. In Table 4, the first three columns present basic information about the set of RR Lyr spectra from Kolenberg et al. (2010) and Fossati et al. (2014) that we used for computing synthetic spectra and constructing our grids of bisectors.

For each spectrum of RR Lyr, we computed the LSD profile as described in Section 4.1 and the bisectors as described in Section 4.2, deriving both $v_{\rm rad}$ and $v_{\rm puls}$ with the same method used for our programme stars. The results are presented in Fig. 6, where the values of the radial velocity and gamma velocity at different phases are indicated with magenta crosses and black squares, respectively. In Table 4, the individual values of radial and gamma velocities and corresponding p-factor values are presented. Moreover, we added some additional Blazhko phases to our test case, in order to check the behaviour of line-profile asymmetries and the performance of the bisectors method in these more difficult phases (see the bottom panel of Fig. 6). We can conclude that, even in the most difficult conditions, we obtain $V_\gamma^{\rm Bis}$ estimates that are fully consistent with those obtained from other phases. The individual estimates of $V_\gamma^{\rm Bis}$ typically lie within the uncertainty of this average value. Our analysis shows that the Blazhko effect does not affect the accuracy of the bisectors method. Indeed, variations in the absolute value of pulsation amplitude should not affect significantly the relative difference of pulsational velocity in different layers of the stellar atmosphere that cause spectral line asymmetry. However, possible non-radial modes that occur in Blazhko stars have to be detected by the method of bisectors in high-resolution and high S/N spectra. The interpretation of non-radial modes in the line-profile asymmetry requires further investigation.

We finally derived an average value of $V_\gamma^{\rm Bis} = -73.9 \pm 5.9$ km s^{-1}. This value is in agreement with literature references obtained with very high-quality data, e.g. $V_\gamma^{\rm RR\,Lyr} = -72.0 \pm 0.5$ km s^{-1} (Chadid 2000). However, in the phase ranges 0.2–0.3 and 0.85–0.90, deviations up to 18 km s^{-1} were found (grey shaded areas in Fig. 6). In these phase ranges, the pulsational velocity is small and our method is not very sensitive to $|v_{\rm puls}| < 5$ km s^{-1}, as will be discussed in the next subsection. Moreover, strong shocks occur in RR Lyrae's atmosphere at phases 0.85–0.9, contributing to the shape of the line profiles, and those phases indeed appear to provide worse performance.

In order to test how flexible the bisectors method is, we derived the gamma velocities for RR Lyr with individual sets of bisector grids for each observation, comparing this with gamma velocities derived using just one bisector grid for all observations. For this test, we chose one bisector grid, number 087, which corresponds to phase

Downloaded from https://academic.oup.com/mnras/article/474/3/3344/4762744 by INAF Trieste (Osservatorio Astronomico di Trieste) user on 01 October 2020

Table 4. Radial velocity measurements for the 41 spectra of RR Lyr from Kolenberg et al. (2010).

Number	Spectrum ID*	Phase	$T_{\rm eff}$**	$v_{\rm obs}^{\rm LSD}$ (km s^{-1})	$\delta v_{\rm obs}^{\rm LSD}$ (km s^{-1})	$v_{\rm puls}$ (km s^{-1})	$v_{\rm puls}/(p$ factor) (km s^{-1})	$V_\gamma^{\rm Bis}$ (km s^{-1})	$\delta V_\gamma^{\rm Bis}$ (km s^{-1})	p factor
1	87	0.173	6325 ± 50	− 93.05	0.87	− 11	− 7.69	− 85.36	2.67	1.43
2	88	0.207	6275 ± 50	− 89.56	0.65	− 11	− 7.74	− 81.83	6.86	1.42
3	89	0.229	6225 ± 50	− 87.27	0.58	− 11	− 7.74	− 79.53	7.76	1.42
4	91	0.260	6175 ± 100	− 83.20	0.59	− 11	− 7.74	− 75.46	6.85	1.42
5	120	0.846	6125 ± 100	− 59.12	1.50	19	15.11	− 74.23	1.50	1.26
6	121	0.868	6375 ± 100	− 67.33	0.95	3	3.02	− 70.35	0.88	0.99
7	122	0.890	6725 ± 100	− 87.20	0.06	− 30	− 22.56	− 64.64	0.69	1.33
8	124	0.922	7050 ± 100	− 108.97	0.67	− 44	− 34.78	− 74.19	2.31	1.27
9	125	0.943	7125 ± 100	− 114.35	0.32	− 50	− 40.54	− 73.81	1.70	1.23
10	126	0.967	7050 ± 100	− 114.00	0.41	− 43	− 33.67	− 80.33	1.31	1.28
11	158	0.604	6000 ± 50	− 57.63	0.56	20	15.95	− 73.58	0.45	1.25
12	160	0.647	6050 ± 50	− 57.26	0.57	21	16.74	− 74.00	0.50	1.25
13	161	0.669	6050 ± 50	− 56.92	0.85	24	19.11	− 76.02	0.78	1.26
14	163	0.698	6025 ± 50	− 56.67	1.01	27	21.51	− 78.19	1.68	1.26
15	164	0.720	6050 ± 50	− 56.78	0.66	26	20.55	− 77.33	0.70	1.26
16	165	0.741	6025 ± 50	− 56.30	0.52	27	21.51	− 77.81	1.44	1.26
17	166	0.763	6000 ± 50	− 55.75	0.61	26	20.57	− 76.32	0.56	1.26
18	168	0.792	6025 ± 50	− 55.04	0.73	26	20.55	− 75.59	0.24	1.26
19	169	0.814	6025 ± 50	− 55.09	1.01	27	21.57	− 76.66	1.23	1.25
20	170	0.834	6050 ± 50	− 56.82	1.55	24	19.09	− 75.90	1.56	1.26
21	171	0.856	6275 ± 75	− 62.12	1.53	20	15.99	− 78.11	1.34	1.25
22	174	0.905	6925 ± 100	− 78.32	0.42	− 25	− 18.90	− 59.42	3.29	1.32
23	175	0.928	7125 ± 75	− 110.98	0.89	− 47	− 38.34	− 72.64	0.37	1.23
24	176	0.948	7125 ± 75	− 113.85	0.06	− 49	− 39.89	− 73.97	0.88	1.23
25	204	0.349	6050 ± 50	− 73.42	1.05	11	8.85	− 82.27	1.61	1.24
26	205	0.372	6000 ± 50	− 71.09	1.13	14	11.04	− 82.13	9.44	1.27
27	206	0.394	5950 ± 75	− 69.65	1.20	17	13.47	− 83.12	0.88	1.26
28	207	0.416	5950 ± 150	− 66.77	1.69	27	21.51	− 88.27	1.68	1.26
29	209	0.452	5975 ± 75	− 63.70	1.43	26	20.57	− 84.27	1.58	1.26
30	210	0.475	5950 ± 75	− 62.56	1.29	20	15.93	− 78.49	2.37	1.26
31	251	0.098	6525 ± 50	− 98.97	0.85	− 21	− 15.61	− 83.36	1.95	1.35
32	252	0.120	6450 ± 50	− 96.71	0.82	− 17	− 12.31	− 84.40	2.10	1.38
33	253	0.141	6400 ± 75	− 94.90	0.78	− 15	− 10.82	− 84.08	1.52	1.39
34	255	0.173	6325 ± 75	− 90.86	0.56	− 19	− 13.90	− 76.95	2.17	1.37
35	256	0.203	6250 ± 50	− 87.01	0.49	− 17	− 12.30	− 74.71	1.65	1.38
36	257	0.226	6200 ± 75	− 85.45	0.74	− 19	− 13.84	− 71.60	0.93	1.37
37	258	0.249	6175 ± 50	− 82.63	0.44	− 17	− 12.18	− 70.46	1.72	1.40
38	260	0.278	6100 ± 50	− 79.65	0.69	− 7	− 4.41	− 75.24	4.33	1.59
39	261	0.303	6050 ± 75	− 76.65	0.91	− 9	− 6.11	− 70.54	1.90	1.47
40	262	0.327	6025 ± 50	− 74.53	1.13	15	12.01	− 86.54	2.30	1.25
41	263	0.349	6025 ± 50	− 72.57	1.23	18	14.17	− 86.74	2.24	1.27

Notes. *IDs of spectra are according to the Kolenberg et al. (2010) and Fossati et al. (2014).
**Effective temperature estimations are from Fossati et al. (2014).

0.173 from our RR Lyrae synthetic models (see Table 4). In Fig. 7, we present the pulsational velocities derived for each spectrum of RR Lyr obtained considering individual grids of bisectors and one bisector grid (ID number 087). The average difference in pulsational velocities along the pulsation curve is relatively small (<3 km s^{-1}), thus we can conclude that the use of only one bisector grid will not affect the final gamma velocity estimations much.

It is worth pointing out that one important ingredient that has a significant impact on the analysis is the microturbulent velocity; different authors (Kolenberg et al. 2010; Fossati et al. 2014) found the need for a depth-dependent value of microturbulence, varying with optical depth in the stellar atmosphere. To take this effect into account, we used the trend found by Fossati et al. (2014) to compute our synthetic spectra. The behaviour of bisector asymmetries computed with depth-dependent $v_{\rm mic}$ stellar atmosphere models and with constant $v_{\rm mic}$ atmosphere models is shown in Fig. 8. As a constant $v_{\rm mic}$ value, we adopt $v_{\rm mic} = 2$ km s^{-1}, following Paper 1. The difference in residual asymmetries is rather large and, as a result, the difference in derived gamma velocities for each individual observation is significant (bottom panel of Fig. 8). It is worth noting that, by using stellar atmosphere models with a depth-dependent microturbulent velocity, the residual accuracy of the derived gamma velocity for RR Lyr is much smaller ($V_{\gamma,\rm RR\,Lyr}^{\rm Bis,depth-dep.}{}^{v_{\rm mic}} = -80.2 \pm 7.8$ km s^{-1}) than the accuracy of the derived gamma velocity based on models with constant $v_{\rm mic}$ ($V_{\gamma,\rm RR\,Lyr}^{\rm Bis,constant}{}^{v_{\rm mic}} = -73.9 \pm 5.9$ km s^{-1}). We can conclude that the current models of depth-dependent microturbulent velocity are not able to reproduce the real observed behaviour of the line-profile asymmetries and the effect of depth-dependent microturbulence velocity requires further theoretical investigation. Our analysis suggests that the use of grids of bisectors

Downloaded from https://academic.oup.com/mnras/article/474/3/3344/4762744 by INAF Trieste (Osservatorio Astronomico di Trieste) user on 01 October 2020

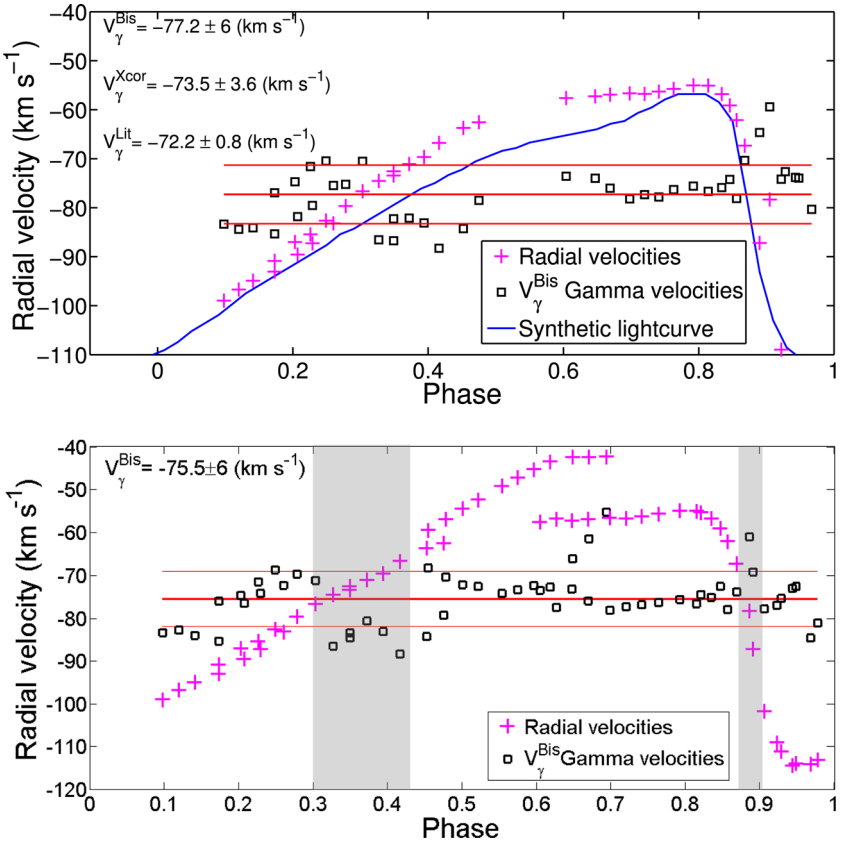

Figure 6. Top panel: gamma velocities of RR Lyr for non-Blazhko phases derived using the method of bisectors (squares), inferred from radial velocity measurements (crosses) at different phases. The template radial velocity curve of RR Lyrae that was using for the Xcor method is drawn as a blue solid line. Bottom panel: the same, including the Blazhko phases. Grey regions presumably correspond to phases with low pulsation velocities, which do not affect the line-profile asymmetry.

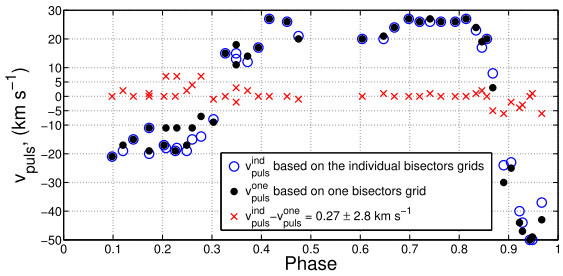

Figure 7. Difference between pulsational velocities for each spectrum of RR Lyr derived with individual sets of bisector grids and one bisector grid, number 087, for all observed spectra.

based on stellar atmospheres with constant v_{mic} velocity should be preferred.

4.4 Accuracy comparison of bisectors and radial velocity curve template methods

One source of uncertainty in this method is that observed spectra are usually taken with finite integration times, which cover a range of phases. The higher the spectral resolution of the observations, the longer the time needed to obtain a good S/N ratio and the larger the *phase-smearing* effect on the observed profile. The use of 4- or 8-m class telescopes alleviates the problem, but it is very difficult to avoid it completely, except for bright stars. The net result is

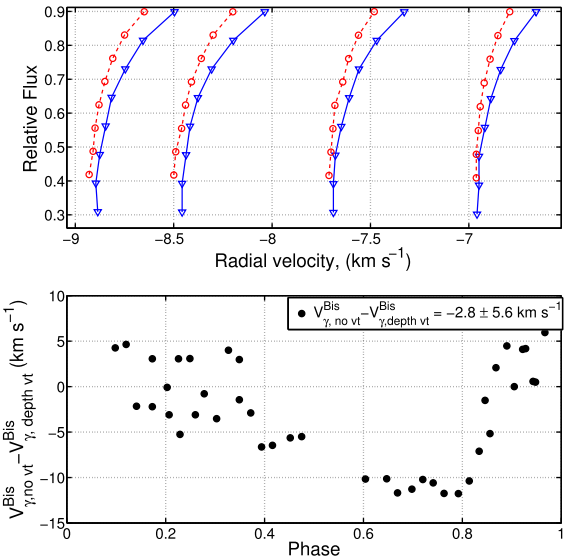

Figure 8. Top panel: comparison of synthetic bisectors computed with the depth-dependent microturbulent velocity model (triangles) and constant microturbulent velocity $v_{mic} = 2\,km\,s^{-1}$ (circles). Bottom panel: difference between the gamma velocities of RR Lyr derived with different sets of bisector grids: with ($V_\gamma^{Bis,depth-dep.v_{mic}}$) and without depth-dependent v_{mic} stellar-atmosphere models ($V_{\gamma,RR\,Lyr}^{Bis,constant\ v_{mic}}$).

Downloaded from https://academic.oup.com/mnras/article/474/3/3344/4762744 by INAF Trieste (Osservatorio Astronomico di Trieste) user on 01 October 2020

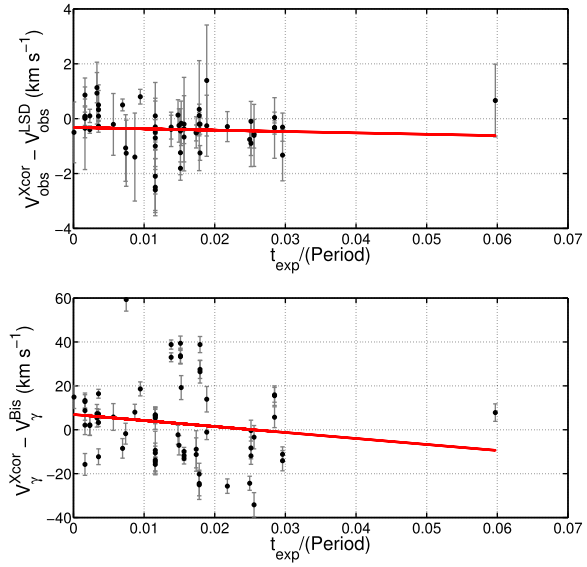

Figure 9. Difference between radial velocities (top panel) and gamma velocities (bottom panel) computed using the cross-correlation method and method of bisectors as a function of the exposure time of observed spectra. The red line in each plot corresponds to the linear fit of investigated values.

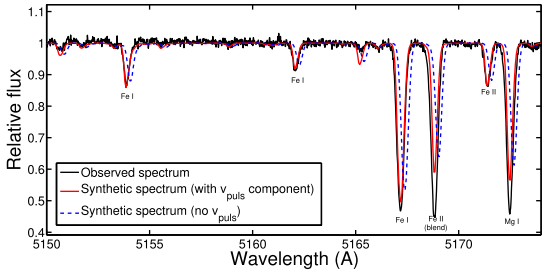

Figure 10. A portion of the spectrum of V Ind observed at phase 0.19 (black solid line) is superimposed on synthetic spectra with (red solid line) and without (blue dashed line) a pulsation velocity component. The synthetic spectra assume the stellar parameters derived in Paper I, i.e. $T_{\rm eff} = 7000$ K, $\log g = 2.3$ dex, $v_{\rm mic} = 1.6$ km s^{-1}. The pulsation velocity determined for this spectrum is -17 km s^{-1}.

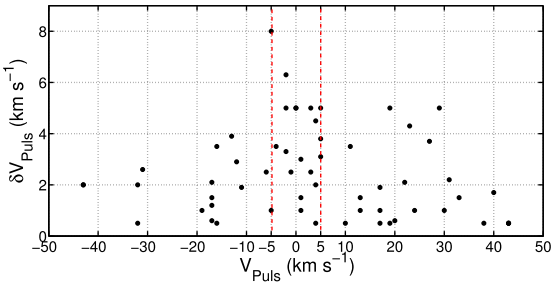

Figure 11. Errors in the pulsational velocity (see text for details) for each observed spectrum at different pulsational velocities.

a general broadening of the observed line profiles compared with the theoretical ones. The smearing should cause subtle shifts in the minimum of the LSD profile – which should reflect on the derived $v_{\rm obs}$ – and subtle changes in the line-profile asymmetries – which should reflect on the derived $v_{\rm puls}$. The size of these effects depends on the phase duration of the exposures, of course. In our sample, we have exposures as long as 45 min (see Paper I), so we tested this hypothesis by comparing the difference between $v_{\rm obs}$ and V_γ obtained with the template-curve method with values obtained with the bisectors method and plotted them as a function of phase coverage in Fig. 9. As can be seen, there is a hint that the bisectors method might underestimate both velocities slightly for increasing phase coverage, but the smearing effect – if any – does not affect the individual errors of the observed radial velocity measurements much. First of all, when the phase smearing gets larger we do not see any significant trend of increasing errors of observed and gamma velocities for the programme stars. Thus, we can conclude that the main sources of the individual errors in observed velocities have a physical and instrumental (resolution and SNR) nature, rather than the smearing effect. For a better understanding of this effect, it is necessary to perform the same analysis with simulated spectra for the given telescope and spectrograph, which requires further study.

Fig. 10 illustrates the quality of our $v_{\rm puls}$ determinations: in spite of the large uncertainties involved in this kind of measurement, the addition of the $v_{\rm puls}$ component brings the synthetic and observed spectra into agreement. Moreover, it can be appreciated that the line shapes are different with and without the inclusion of the pulsation velocity.

The resulting $v_{\rm puls}^{\rm Bis}$ determinations, with their errors $\delta v_{\rm puls}^{\rm Bis}$, are reported in Table 3, along with the final V_γ and its propagated error, δV_γ. The errors in the pulsational velocity ($\delta v_{\rm puls}^{\rm Bis}$) have been computed as the standard deviation of measurements $v_{\rm puls}^{\rm Bis}$ obtained from the fit of different parts of the theoretical and observed bisectors, considering that LSD profiles can be distorted by blends. Thus, for each observation, we measured the pulsational velocities by using a different number of LSD profile layers: namely we cut the bisectors at the fourth, fifth, sixth and seventh layers and derived a different $v_{\rm puls}$ for each cut. In this way, we tested how reliable bisectors are in reflecting the asymmetries of LSD profiles. The results are plotted in Fig. 11, as a function of the pulsational velocity of each individual exposure. As can be seen, the errors are always below 5 km s^{-1}, with a typical (median) value of 1.5 km s^{-1}, except for a narrow range of pulsational velocities, from –5 to +5 km s^{-1}, with a median value of 3.5 km s^{-1}. The comparably higher scatter that is obtained for pulsational velocities having smaller values is connected with the intrinsic sensitivity of the method: (i) blends do affect the shape of the LDS profile and (ii) the asymmetry of the profile tends to vanish for small pulsation velocities and consequently the error in its determination increases. This behaviour of $\delta v_{\rm puls}^{\rm Bis}$ constrains the range of reliable application of the LSD method and has an impact on the gamma velocity error, δV_γ.

Fig. 12 compares the final V_γ obtained with the classical and bisector methods. As can be seen, stars that do not possess reliable observed curves in the literature (for example from the Baade–Wesselink method) have a larger difference, caused mostly by uncertainties in the classical template-fitting method. If we limit the comparison to stars having reliable template radial velocity curves, we can see an overall agreement at the level of $\Delta V_\gamma = -0.1 \pm 10.7$ km s^{-1}.

We also note that the most discrepant stars (marked in grey in Fig. 12) are observed with SARG and generally have lower S/N ratios and a larger phase coverage (smearing), because it is mounted on a 4 m-class telescope, while the UVES spectra produce less scattered results.

Another way to study *a posteriori* the error of the whole method consists of evaluating the spread in repeated V_γ measurements for the same star, when more than one determination was available. We found a typical spread of –10 to +10 km s^{-1}, with the maximum variations generally corresponding to phase ranges 0.4–0.5. Fig. 13

Downloaded from https://academic.oup.com/mnras/article/474/3/3344/4762744 by INAF Trieste (Osservatorio Astronomico di Trieste) user on 01 October 2020

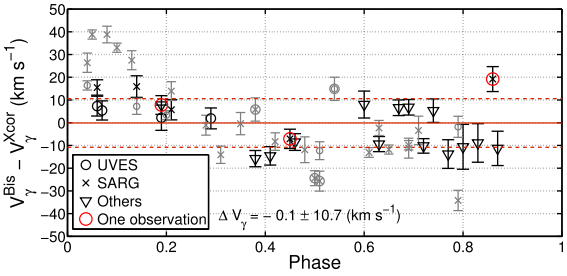

Figure 12. Difference between gamma velocities derived with the radial velocity curve template ($V_\gamma^{\rm Xcor}$) and the LSD profile asymmetry method ($V_\gamma^{\rm Bis}$). Observations from different spectrographs are labelled respectively and stars that have only one epoch spectrum are also marked. Stars marked in black are those having reliable observed radial velocity curves in the literature (e.g. from the Baade–Wesselink method), while stars marked in grey have $V_\gamma^{\rm Xcor}$ derived from less reliable templates.

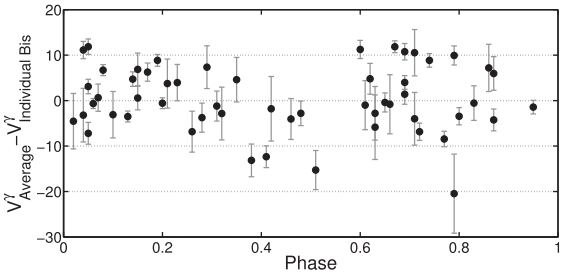

Figure 13. The difference of $V_\gamma^{\rm Bis}$ of individual exposures with the average V_γ for each star as a function of phase.

shows the difference in V_γ measurements obtained from individual exposures with the average V_γ of each star, as a function of phase. No systematic trends are apparent and the spread is generally consistent with the estimated errors.

4.5 Projection factor

When deriving radial velocities from absorption-line profiles, either with cross-correlation or with LSD profiles, the information is implicitly integrated over the stellar surface and along the radius of the pulsating star. Such integration is affected by limb-darkening across the stellar surface and by radial velocity gradients with depth in the atmosphere of the star, where lines form. Both effects depend on the pulsation phase (Marengo et al. 2003) and therefore they are generally modelled as follows:

$$p = v_{\rm puls}/(v_{\rm rad} - V_\gamma), \qquad (2)$$

also known as the projection factor, or the factor by which one should multiply the observed radial velocity (in the line of sight) to obtain the intrinsic pulsational velocity of the star (along the radial direction), corrected by projection effects.

The projection factor becomes very important in the Baade–Wesselink method, where a relatively small error in pulsation velocity may lead to a large error in distance. The first works by Eddington (1926) or Carroll (1928) lead to an estimate of $p = 1.41$, which was used in many Baade–Wesselink studies of Cepheids, to correct for limb-darkening and radial velocity expansion effects on the derived distances. Later, different values were proposed, ranging from 1.2–1.4 (see Nardetto et al. 2014, for a review). For the closest stars, it is possible to measure the projection factor directly, with the help of interferometric observations (e.g. Breitfelder

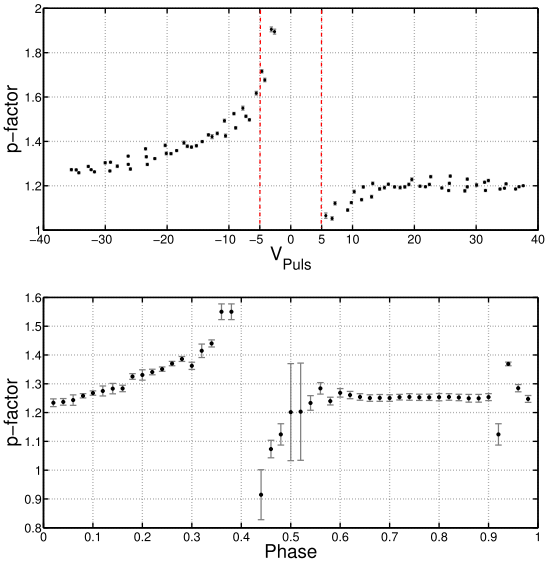

Figure 14. Model behaviour of the p factor with different pulsation velocity (top panel) and different phase (bottom panel). We plotted the average values of the projection factor for each value of the modelled pulsational velocity, over all 41 bisector grids (see Appendix A). The vertical dashed lines in the top panel mark the limits of applicability of our method (from –5 to +5 km s^{-1}; also see Fig. 11), which correspond roughly to the phase range 0.35–0.50.

et al. 2015). An investigation with realistic hydrodynamical models of δ Cep by Nardetto et al. (2004, see also the subsequent work by Nardetto et al. 2013, 2014, 2017) showed that projection effects can be corrected with residuals below $\simeq$1 km s^{-1} and that the appropriate projection factor depends on the method used to derive the projected pulsational velocity.

In our case, the projection factor was computed using the bisectors method (an application to Cepheids can be found in Sabbey et al. 1995). We modelled the theoretical line profiles by taking into account the geometrical effect (limb-darkening) for each model that we have used for calculations in our library of bisectors. The particularity of our approach is that we are using the average profiles of different spectral lines (via the LSD technique) in order to investigate the clear geometrical effect of radial pulsations.

In more detail, we used the 41 existing models for RR Lyrae over all pulsation phases from Fossati et al. (2014); see Appendix A for more details. For each model, corresponding to a different phase, we computed a set of synthetic spectra with pulsation velocities ranging from −50 km s^{-1} to +50 km s^{-1} with a step of 1 km s^{-1}, in the same wavelength range used for our $v_{\rm obs}$ measurements, 5100–5400 Å (see Fig. 4). We then computed $v_{\rm obs}$ and $v_{\rm puls}$, as done for the observed spectra in our sample. We can then compute the projection factor using equations (1) and (2). In Fig. 14, we illustrate the behaviour of our modelled p factor – obtained from our grids of model bisectors (Appendix A) – versus pulsational velocity and phase. The top panel clearly shows the limits of applicability of the bisectors method, which loses sensitivity in the −5 km s^{-1} to +5 km s^{-1} range, as also discussed previously. As a comparison, we repeated the same analysis using just the Mg I triplet lines (5167.321, 5172.684, 5183.604 Å) instead of all prominent lines from our initial line list. In this case we built the synthetic grid of bisectors and derived the observed ones for our stellar sample based only on these three lines. The Mg triplet is a prominent feature in the spectra of RR Lyraes and it allowed us to test our p-factor

Downloaded from https://academic.oup.com/mnras/article/474/3/3344/4762744 by INAF Trieste (Osservatorio Astronomico di Trieste) user on 01 October 2020

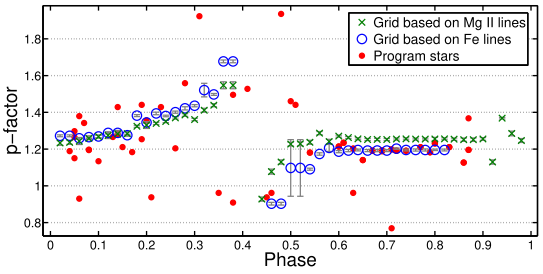

Figure 15. Observed behaviour of the p factor with different phases for a sample of programme spectra (red dots). As a reference, theoretical values of the p factor are labelled by blue circles and green crosses, based on the LSD profiles of synthetic spectra for all lines in the range 5100–5400 Å (circles) and the Mg I triplet lines only (crosses).

modelling under different conditions (less numerous but stronger lines; see Fig. 15).

In order to investigate the effect of the behaviour of the projection factor on our sample of real stars, we repeated the same procedure to derive the p factor of the observed LSD profiles for the whole sample of stars. We can also plot the *observedp* factor for each of the analysed spectra, illustrated in Fig. 15. Considering that we used the same bisectors library, we expect to obtain roughly the theoretical behaviour illustrated in the lower panel of Fig. 14, modulated by the fitting uncertainties. While globally this is true, there are several outliers, which we can see in Fig. 15, in some cases displaying totally unrealistic values of the p factor, for example $p < 1$ and $p > 1.6$. This is most likely caused by measurement uncertainties in the derived $v_{\rm puls}$, caused by line smearing, low S/N, blends and other observational effects and discussed in the previous section. However, the overall behaviour of p factors derived from the observed profiles of our sample stars appears to agree well with that obtained from the models based on RR Lyrae. This confirms the overall self-consistency of our analysis. The comparison of p factors derived from our whole line list and from the Mg triplet shows a small offset that varies with phase (up to 0.07). We conclude that line selection can have a noticeable impact on the actual p-value derivation. When the offset is compared with the $v_{\rm obs}$ spread, however, it becomes largely irrelevant.

It should be noted that, in the framework of our analysis, we assume that all lines, even those with different individual depths, behave in the same way – i.e. the shape of all spectral features is the same at given pulsational velocity. This is not a fully correct assumption; however, the primary goal of this article is to develop a method that can give reliable estimations of the gamma and pulsational velocities from just one spectral observation. For this reason, using a few prominent lines or a list of many weak lines is equally good for deriving investigated velocities.

5 DISCUSSION

The final velocity measurements for each star with the two methods were obtained as averages of the single-epoch gamma determinations listed in Tables 2 and 3, respectively, and are listed in Table 5 along with their errors. The comparison between the two methods was already discussed in Section 4 (see Figs 9 and 12). Here, we will compare our results with the available literature. We will also discuss in more depth the uncertainties and applicability of the bisectors method to the derivation of gamma velocities for pulsating stars.

Table 5. Final results for the programme stars, obtained with both the cross-correlation and bisectors methods.

Star	$V_\gamma^{\rm Xcor}$ (km s^{-1})	$\delta V_\gamma^{\rm Xcor}$ (km s^{-1})	$V_\gamma^{\rm Bis}$ (km s^{-1})	$\delta V_\gamma^{\rm Bis}$ (km s^{-1})
DR And	− 119	9	− 110	4
X Ari*	− 36	5	− 44	6
TW Boo	− 100	2	− 89	2
TW Cap*	− 72	6	− 87	6
RX Cet*	− 94	5	− 68	6
U Com	− 7	4	− 19	6
RV CrB	− 140	4	− 133	5
UZ CVn	− 18	4	− 49	6
SW CVn	21	7	14	6
AE Dra	− 276	2	− 311	5
BK Eri	97	4	93	11
UY Eri*	152	6	146	7
SZ Gem*	322	5	346	6
VX Her	− 371	5	− 352	10
DH Hya	334	5	348	18
V Ind	197	3	200	9
SS Leo	164	5	157	2
V716 Oph*	− 311	6	− 370	6
VW Scl	40	4	36	13
BK Tuc	170	5	134	7
TU UMa*	99	5	106	7
RV UMa	− 198	5	− 175	6
UV Vir*	99	5	81	6

Note. * For these stars, only one spectrum was obtained.

5.1 Literature comparisons

We report in Table 6 our literature search for radial and gamma velocity measurements of the programme stars ($V_\gamma^{\rm Lit}$). We compare the gamma velocities obtained in the literature with our measurements obtained with both methods in Fig. 16. As can be seen, both the classical method (top panel) and the bisector method (bottom panel) produce results that are generally compatible with the literature, within the quoted uncertainties, with a few exceptions.

We note that for the most discrepant cases, like AE Dra, UZ CVn or BK Eri, the discrepancy with the literature persists regardless of the method employed, suggesting that perhaps there is a problem with those specific stars. The spectra of SW CVn and RV CrB have low S/N ratio ($\leq$50) and they were excluded from the abundance analysis in Paper I; however, we included them in this work, because the S/N ratio was sufficient for radial velocity analysis. These stars were included here because the S/N ratio was sufficient to produce reliable radial velocity estimates and indeed they agree with the literature with both methods. The spectra of AE Dra have good S/N ratios, but they suffer from some phase smearing because they were observed for 30 and 45 min and this is reflected in their large error bars, which make them only marginally incompatible with the literature. The spectra of BK Eri have quite high S/N and short exposure times, so we suspect that in this case the problem might lie in the literature measurements. Finally, there are two stars that show values marginally discrepant with the literature and from one method to the other: SZ Gem and BK Tuc. SZ Gem has only one spectrum and this can pose a problem of non-reliable template curve fitting or a non-sensitive regime of pulsation phases in the bisectors method – between –5 km s^{-1} and +5 km s^{-1}. Indeed, the derived pulsational velocity for this spectrum is relatively small, 13 km s^{-1} at phase 0.50. BK Tuc was observed in three exposures of 30 min each, which might introduce some phase smearing of the line profiles.

Downloaded from https://academic.oup.com/mnras/article/474/3/3344/4762744 by INAF Trieste (Osservatorio Astronomico di Trieste) user on 01 October 2020

Table 6. Summary of literature results for the programme stars, for both observed heliocentric radial velocity estimates ($v_{\rm rad}$) and gamma velocities (V_γ), along with their errors, when available.

Star	$v_{\rm rad}^{\rm Lit}$ (km s^{-1})	$\delta v_{\rm rad}^{\rm Lit}$ (km s^{-1})	Ref	$V_\gamma^{\rm Lit}$ (km s^{-1})	$\delta V_\gamma^{\rm Lit}$ (km s^{-1})	Ref
DR And	– 81	30	(1)	– 103.6	2.0	(3)
X Ari*	– 36	1	(1)	– 41.6	3	(4)
TW Boo	– 99	1	(1)	– 99	5	(5)
TW Cap	– 32	1	(1)	...	...	
RX Cet	– 57	2	(1)	...	...	
U Com*	– 22	3	(1)	– 18	3	(6)
RV CrB	– 125	5	(1)	– 125	5	(7)
UZ CVn*	– 28	3	(1)	– 27	10	(6)
SW CVn	– 18	21	(1)	– 18	21	(8)
AE Dra	– 243	30	(1)	– 243	30	(8)
BK Eri	141	10	(1)	141	10	(7)
UY Eri	171	1	(1)	...	...	
SZ Gem	326	4	(1)	305	15	(5)
VX Her*	– 377	3	(1)	– 361.5	5	(4)
DH Hya	355	8	(1)	355	8	(7)
V Ind*	202	2	(1)	202.5	2	(9)
SS Leo*	144	7	(2)	162.5	6.8	(10)
V716 Oph	– 230	30	(1)	– 230	5	(11)
VW Scl	53	10	(1)	53	10	(12)
BK Tuc	121	14	(1)	121	14	(7)
TU UMa*	89	2	(1)	101	3	(13)
RV UMa	– 185	1	(1)	– 185	1	(7)
UV Vir	99	11	(1)	99	11	(7)

Notes. *These stars were studied with the Baade–Wesselink method.
Literature references: (1) Beers et al. (2000); (2) Kordopatis et al. (2013); (3) Jeffery et al. (2007); (4) Nemec et al. (2013); (5) Hawley & Barnes (1985); (6) Fernley & Barnes (1997); (7) Dambis (2009); (8) Layden (1994); (9) Clementini et al. (1990); (10) Carrillo et al. (1995); (11) McNamara & Pyne (1994); (12) Solano et al. (1997); (13) Preston & Spinrad (1967).

If we exclude the three most problematic stars, both methods compare quite well with the literature, with the following weighted average differences: $\Delta V_\gamma^{\rm Xcor} = -3 \pm 20$ km s^{-1} and $\Delta V_\gamma^{\rm Bis} = -3 \pm 30$ km s^{-1}, where the differences are computed as our measurements minus the literature ones. The observed spreads are marginally incompatible with the uncertainties typically quoted, which are 5, 12 and 7 km s^{-1} for the cross-correlation method, the bisectors method and the literature collection, respectively. The uncertainties quoted for the different methods are rather compatible with each other, suggesting that there must be some error source that has been unaccounted for in *all* of the methods. If so, the unaccounted-for error source amounts to 10–20 km s^{-1} in each method. Systematic errors of this amplitude are easy to accommodate when one applies template curve fitting to just a few measurements, as in our case. These errors are also easy to accommodate, at least for the noisiest spectra, into the bisectors method sensitivity. On the other hand, we are comparing our data with literature results that are derived with several different methods and data samples, so the inhomogeneity of the comparison measurements certainly plays an important role. An explanation of this general spread in the comparison of gamma velocities with literature values can likely be found in the fact that the stars for which B–W analysis was performed have a difference in this comparison less than or equal to 10 km s^{-1} in both $V_\gamma^{\rm Xcor} - V_\gamma^{\rm Lit}$ and $V_\gamma^{\rm LSD} - V_\gamma^{\rm Lit}$ values. It is a rather small difference and the reason for this is actually that these stars have reliable radial velocity curves based on the B–W method. As a result, the $V_\gamma^{\rm Xcor}$ are more reliable as well, because the light-curve analysis was based on the same radial velocity curves as in the B–W method. Moreover, in Fig. 12 we can see the same behaviour of the difference $V_\gamma^{\rm Xcor} - V_\gamma^{\rm LSD}$ – the stars for which the B–W method was applied in the literature have less scatter in the gamma velocity.

We can conclude, after considering the literature comparison with stars having reliable radial velocity curves, that the bisectors method performs at least as well as the more traditional template curve technique.

6 CONCLUSIONS

We perform a systematic study of the radial velocities for a sample of 23 variable stars – mostly RRab, with two RRc and three W Vir – using high-resolution spectra from both proprietary (UVES and SARG) and archival (UVES, HARPS, FEROS, APO) data sets.

For each star, we derive the radial velocity using two independent methods: the cross-correlation approach and the LSD profile technique. The errors of individual estimates of radial velocity in both methods are on the level of ± 2 km s^{-1} or less. The determination of gamma velocities was also performed with two methods, the first based on the classical radial velocity curve template technique and the second on line-profile asymmetries, referred to as the bisectors method (see Section 4.2). With the help of LSD technique, we provide and test a method for determining the pulsation and gamma velocity of pulsating variable stars when only scarce observations taken at random phases are available. We also computed a grid of synthetic bisectors for each of 41 phases (see Appendix A), which is made available electronically. Our public library can be used in the general case to make an assumption about the velocity of the barycentre of pulsating stars, in the best case to within an error of ± 5 km s^{-1}.

In summary, the method of deriving gamma velocities of RR Lyraes presented here has the following milestones.

(i) The method is working well for radially pulsating stars: RRab Lyraes and classical Cepheids; to quantify the level of line-profile asymmetry, we used the average profile of different spectral lines (the LSD profile).

(ii) The method is phase sensitive, with the best accuracy derived at phases 0–0.2 and 0.5–0.85; at these phases the pulsation velocity is large, thus the line-profile asymmetry is easier to identify.

(iii) The shock phases during the pulsation cycle in RRab stars do affect the accuracy of the method, mostly at phases 0.85–0.95, when the line-profile geometry changes dramatically.

(iv) The method is working with both low- and high- S/N spectra; the spectral resolution at which we applied the method was about $R \approx 30\,000$.

(v) The major advantage of the method is that it can derive the gamma velocity of a star just from one observation, or from observations taken at unknown phase; however, the accuracy of the method depends on many factors. We estimated the average error of the determined pulsational velocity as $\delta v_{\rm puls} \approx 3.5$ km s^{-1} and the residual error of the gamma velocity as $\delta V_\gamma^{\rm Bis} \approx 10$ km s^{-1}.

ACKNOWLEDGEMENTS

We thank the anonymous referee for helpful comments, which improved the article significantly. NB acknowledges partial support under MINECO projects AYA2015-68012-C2-1-P and SEV 2015-0548 and also warmly thanks Gisella Clementini and Carla Cacciari for useful recommendations during work on this article and all at the INAF–Bologna Observatory, where most of this work was carried out, for hospitality during the grant stay. DR acknowledges financial

Downloaded from https://academic.oup.com/mnras/article/474/3/3344/4762744 by INAF Trieste (Osservatorio Astronomico di Trieste) user on 01 October 2020

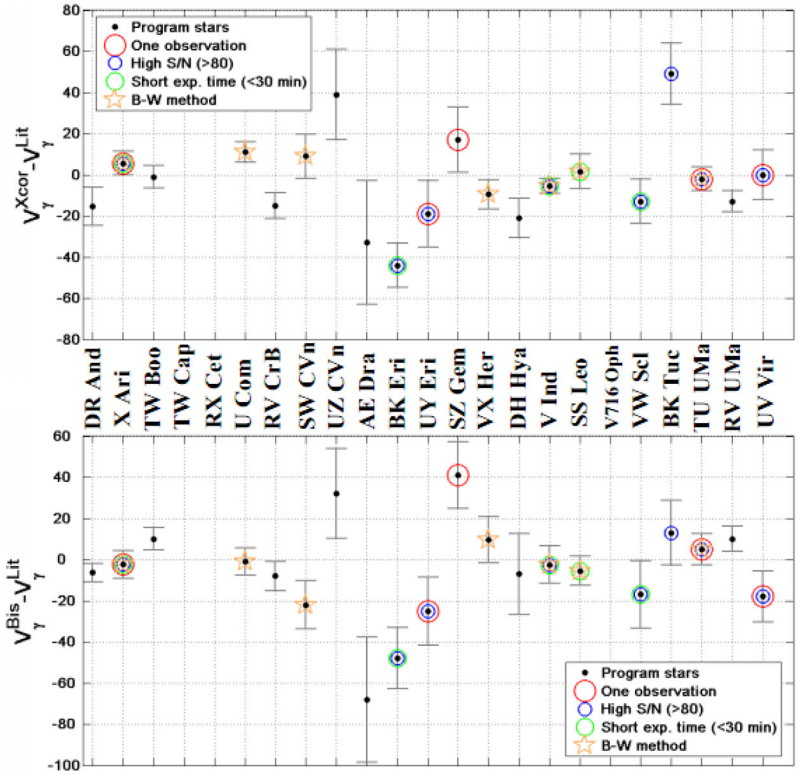

Figure 16. Differences between our measurements and literature ones. Top panel: difference between gamma velocities from the cross-correlation method and template curve fitting ($V_\gamma^{\rm Xcor}$) with the literature ($V_\gamma^{\rm Lit}$). Bottom panel: difference between the gamma velocity from LSD profiles and bisectors ($V_\gamma^{\rm LSD}$) with the literature. We marked the stars by different colours, taking into account some relevant characteristics of their spectra: stars that have only one measurement (red), short exposure times (green), high SNR (blue) and Baade–Wesselink literature estimates (orange).

support from PRIN MIUR 2010–2011, project 'The chemical and dynamical evolution of the Milky Way and Local Group galaxies', prot. 2010LYSN2T. VT acknowledges partial support by RFBR, research project No.15-52-12371. In this work we made extensive use of the NASA ADS abstract service, the Strasbourg CDS data base and the atomic data compiled in the VALD data base.

This work was based on data collected with UVES@VLT under programme ID 083.B-0281 and with SARG@TNG under programme IDs AOT 19 TAC 11 and AOT 20 TAC 83. Also based on ESO FEROS and HARPS archival reduced data products, under programme IDs 079.D-0462 and 178.D-0361. Also based on data of RR Lyrae obtained with the 2.7-m telescope at the McDonald Observatory, TX, USA.

REFERENCES

Ballester P., Modigliani A., Boitquin O., Cristiani S., Hanuschik R., Kaufer A., Wolf S., 2000, The Messenger, 101, 31
Beers T. C., Chiba M., Yoshii Y., Platais I., Hanson R. B., Fuchs B., Rossi S., 2000, AJ, 119, 2866
Benedict G. F. et al., 2011, AJ, 142, 187
Breitfelder J., Kervella P., Mérand A., Gallenne A., Szabados L., Anderson R. I., Willson M., Le Bouquin J.-B., 2015, A&A, 576, A64
Cacciari C., Clementini G., Prevot L., Lindgren H., Lolli M., Oculi L., 1987, AJ, 69, 135
Carrillo D., Burki G., Mayor M., Burnet M., Lampens P., Nicolet B., 1995, A&AS, 113, 483
Carroll J. A., 1928, MNRAS, 88, 548
Chadid M., 2000, A&A, 359, 991
Chadid M., Vernin J., Gillet D., 2008, A&A, 491, 537
Clementini G., Cacciari C., Lindgren H., 1990, A&A, 85, 865
Dambis A. K., 2009, MNRAS, 396, 553
Dekker H., D'Odorico S., Kaufer A., Delabre B., Kotzlowski H., 2000, SPIE, 4008, 534
Donati J.-F., Semel M., Carter B. D., Rees D. E., Collier Cameron A., 1997, MNRAS, 291, 658
Eddington A. S., 1926, The Internal Constitution of the Stars, Cambridge: Cambridge University Press
Fernley J., Barnes T. G., 1997, A&AS, 125, 313
For B.-Q., Sneden C., Preston G. W., 2011, ApJS, 197, 29
Fossati L., Kolenberg K., Shulyak D. V., Elmasli A., Tsymbal V., Barnes T. G. Guggenberger E., Kochukhov O., 2014, MNRAS, 445, 4094
Gaia Collaboration et al., 2016, A&A, 595, A1
Gratton R. G. et al., 2001, ExA, 12, 107
Gray D. F., 2010, ApJ, 721, 670
Guggenberger E., Shulyak D., Tsymbal V., Kolenberg K., 2014, IAU Symposium, 301, 261
Hareter M., Kochukhov O., Lehmann H., Tsymbal V., Huber D., Lenz P., Weiss W. W., Matthews J. M., 2008, A&A, 492, 185
Hatzes A. P., 1996, PASP, 108, 839
Hawley S. L., Barnes T. G., III, 1985, PASP, 97, 551
Jeffery E. J., Barnes T. G., III, Skillen I., Montemayor T. J., 2007, ApJS, 171, 512
Jones R. V., Carney B. W., Latham D. W., Kurucz R. L., 1987, AJ, 312, 254
Jones R. V., Carney B. W., Latham D. W., 1988, AJ, 326, 312
Kochukhov O., Makaganiuk V., Piskunov N., 2010, A&A, 524, A5
Kolenberg K., Fossati L., Shulyak D, Pikall H., Barnes T. G., Kochukhov O., Tsymbal V., 2010, A&A, 519, A64
Kollmeier J. A. et al., 2009, ApJ, 705, 158
Kordopatis G., Gilmore G., Steinmetz M., Boeche C., Seabroke G. M., Siebert A., Zwitter T., 2013, AJ, 146, 134
Kurucz R, 1993, CD-ROM No. 18. Smithsonian Astrophysical Observatory, Cambridge, MA

Downloaded from https://academic.oup.com/mnras/article/474/3/3344/4762744 by INAF Trieste (Osservatorio Astronomico di Trieste) user on 01 October 2020

Layden A. C., 1994, AJ, 108, 1016
Liu T., 1991, PASP, 103, 205
Liu T., Janes K. A., 1989, AJ, 69, 593
Maas T., Giridhar S., Lambert D. L., 2007, AJ, 666, 378
Marengo M., Karovska M., Sasselov D. D., Papaliolios C., Armstrong J. T., Nordgren T. E., 2003, ApJ, 589, 968
McNamara D. H., Pyne M. D., 1994, PASP, 106, 472
Moskalik P. et al., 2015, MNRAS, 447, 2348
Mucciarelli A., Pancino E., Lovisi L., Ferraro F. R., Lapenna E., 2013, ApJ, 766, 78
Nardetto N., Fokin A., Mourard D., Mathias P., Kervella P., Bersier D., 2004, A&A, 428, 131
Nardetto N., Stoekl A., Bersier D., Barnes T. G., 2008, A&A, 489, 1255
Nardetto N., Mathias P., Fokin A., Chapellier E., Pietrzynski G., Gieren W., Graczyk D., Mourard D., 2013, A&A, 553, A112
Nardetto N., Storm J., Gieren W., Pietrzyński G., Poretti E., 2014, IAU Symposium, Precision Asteroseismology, Vol. 301, p. 145
Nardetto N., Poretti E., Rainer M., Guiglion G., Scardia M., Schmid V. S., Mathias P., 2014, A&A, 561, A151
Nardetto N. et al., 2017, A&A, 597, A73
Nemec J. M., Cohen J. G., Ripepi V., Derekas A., Moskalik P., Sesar B., Chadid M., Bruntt H., 2013, ApJ, 773, 181
Pancino E., Britavskiy N., Romano D., Cacciari C., Mucciarelli A., Clementini G., 2015, MNRAS, 447, 2404 (Paper I)
Preston G. W., Spinrad H., 1967, ApJ, 147, 1025
Sabbey C. N., Sasselov D. D., Fieldus M. S., Lester J. B., Venn K. A., Butler R. P., 1995, ApJ, 446, 250
Samus N. N., Kazarovets E. V., Durlevich O. V., Kireeva N. N., Pastukhova E. N., 2017, General Catalogue of Variable Stars: Version GCVS 5.1, Astronomy Reports, Vol. 61, No. 1, pp. 80
Sanford R. F., 1952, ApJ, 116, 331
Sessar B., 2012, AJ, 144, 114
Skarka M., 2013, A&A, 549, A101
Solano E., Garrido R., Fernley J., Barnes T. G., 1997, A&AS, 125, 321
Stetson P. B., Pancino E., 2008, PASP, 120, 1332
Stetson P. B., Fiorentino G., Bono G., Bernard E. J., Monelli M., Iannicola G., Gallart C., Ferraro I., 2014, PASP, 126, 616
Tkachenko A., Van Reeth T., Tsymbal V., Aerts C., Kochukhov O., Debosscher J., 2013, A&A, 560, A37
Tonry J., Davis M., 1979, AJ, 84, 1511
Tsymbal V. V., 1996, in Adelman S. J., Kupka F., Weiss W. W., eds, ASP Conf. Ser. Vol. 108, Model Atmospheres and Spectrum Synthesis. Astron. Soc. Pac., San Francisco, p. 198
Van Reeth T., Tkachenko A., Tsymbal V., 2013, EAS Publ. Ser., 64, 237
Wallerstein G., 1958, ApJ, 127, 583

SUPPORTING INFORMATION

Supplementary data are available at *MNRAS* online.

Table A1. The grids of synthetic bisectors.

Please note: Oxford University Press is not responsible for the content or functionality of any supporting materials supplied by the authors. Any queries (other than missing material) should be directed to the corresponding author for the article.

APPENDIX A: GRIDS OF SYNTHETIC BISECTORS

We publish a grid of synthetic bisectors that can be used to compute the pulsational velocity of any observed spectrum of radial pulsating variables of the RRab Lyrae type and Cepheids with the method described in Section 4. Due to the small number of RRc variables (only two) in our sample, we could not make statistically significant conclusions about application of the method to this type of variable. The grid contains one set of bisectors (from -50 to $+50\,\mathrm{km\,s^{-1}}$ with a step of $1\,\mathrm{km\,s^{-1}}$ of pulsational velocity variation) for each of the 41 different phases computed on the basis of the individual atmospheric models along the pulsation cycle of RR Lyr. Each individual atmospheric model was based on the stellar parameters derived in Fossati et al. (2014) and phase coverage is presented in Table 4. The IDs of each bisector grid correspond to the IDs of the atmospheric models from Fossati et al. (2014).

In order to build the grid of bisectors, we followed the next steps. For each of the 41 selected phases, we computed a set of synthetic spectra in the same wavelength range used for the radial velocity measurements (5100–5400 Å) with the STARSP-SYNTHV code (Tsymbal 1996), based on the ATLAS9 model atmospheres. We used the last modification of the code, which for the construction of line profiles took into account stellar radial pulsations, individual chemical abundances and depth-dependent microturbulent velocity for a given star. For the calculations, we adopt a constant microturbulent velocity of $2\,\mathrm{km\,s^{-1}}$. However, as discussed at the end of Section 4.3, the choice of one bisector grid for the analysis of all observed spectra will have no effect on the accuracy of the final gamma velocity measurements. For each synthetic spectrum, we computed the LSD profile and its bisector, using exactly the same method adopted for the observed spectra (Section 4). The resulting sets of bisectors serves us as a final library of bisectors.

The grid is published in the electronic version of the journal and at CDS; Table A1 provides an example of its contents. To be able to use the grid, the set with the phase closest to the observed one needs to be selected and then the bisector's points need to be scaled to the actual resolution of the observed spectra, by multiplying the X_n coordinates of the eight bisector points by $\mathrm{FWHM_{LSD}}/\mathrm{FWHM_{obs}}$, where $\mathrm{FWHM_{LSD}}$ is the full width at half-maximum of the synthetic bisector, reported in the last column of Table A1, while $\mathrm{FWHM_{obs}}$ is the value obtained for the observed spectra.

A general suggestion is that, to make a more accurate determination of the centre-of-mass velocity of radial pulsating Cepheids and RR Lyraes, it is better to use individual grids of synthetic bisectors. Since the line-profile asymmetry depends on atmospheric parameters, in ideal situation it is necessary to build the grid of synthetic spectra with T_{eff}, $\log g$ and v_{mic} for a particular star, but the values provides can be used for stars that are not too different from RR Lyrae.

Downloaded from https://academic.oup.com/mnras/article/474/3/3344/4762744 by INAF Trieste (Osservatorio Astronomico di Trieste) user on 01 October 2020

Table A1. The grids of synthetic bisectors. The names of each file corresponds to the spectrum ID of that phase by Fossati et al. (2014). The columns contain the following: (1) the intrinsic pulsational velocity $v_{\rm puls}$ of the bisector points; (2) the difference $v_{\rm rad} - V_\gamma$, or in other words the observed pulsational velocity *uncorrected for projection effects*, see equation (2); (3)–(10) the X_n coordinates of the eight bisector points, or in other words the centres of the bisectors in radial velocity space, expressed as offsets from the gamma velocity (zero by definition, in this system); (11)–(18) the Y_n coordinates of the eight bisector points, expressed in terms of relative flux (where 1 is the continuum and 0 full absorption); (19) the full width at half-maximum (FWHM) of the synthetic LSD profile (see text). The table is available in its entirety in the electronic version of the journal and at CDS. Only the first five rows are reported here, for guidance regarding its form and content.

$v_{\rm puls}$ km s^{-1}	$v_{\rm rad} - V_\gamma$* km s^{-1}	$X1$ km s^{-1}	... ...	$X8$ km s^{-1}	$Y1$ (per cent)	... ...	$Y8$ (per cent)	FWHM Å
–45	−35.43	0.32	...	3.53	0.67	...	0.91	23.30
–44	−34.65	0.37	...	3.49	0.66	...	0.91	22.92
–43	−34.21	0.42	...	4.24	0.68	...	0.91	23.90
–42	−32.67	0.29	...	3.56	0.67	...	0.91	23.06
–41	−32.25	0.27	...	3.62	0.65	...	0.91	21.78

Notes. *The accuracy in the estimation of observed synthetic pulsational velocities ($v_{\rm rad} - V_\gamma$) corresponds to the accuracy of finding the minimum of the appropriate LSD profile (i.e. $\delta v_{\rm obs}^{\rm LSD}$), see Section 4.1.

This paper has been typeset from a TEX/LATEX file prepared by the author.

Downloaded from https://academic.oup.com/mnras/article/474/3/3344/4762744 by INAF Trieste (Osservatorio Astronomico di Trieste) user on 01 October 2020